On the closed-loop stochastic dynamics of two-state nonlinear exothermic CSTRs with PI temperature control

Jesus Alvarez[a] and Roberto Baratti[b]*

[a] Universidad Autónoma Metropolitana
Departamento de Ingeniería de Procesos
09340 México City, México

[b] Università degli Studi di Cagliari
Dipartimento di Ingegneria Meccanica, Chimica e Materiali
Cagliari I-9123, Italy

Abstract

The closed-loop (CL) 3-state stochastic dynamics of a benchmark 2-state nonlinear (NL) exothermic continuous reactor class with linear proportional-integral (PI) temperature control is analyzed with Fokker Planck (FP) partial differential equation (PDE) theory. The geometric correspondence between the CL stationary state probability density function (PDF) and deterministic global monostability is established. A control gain condition to attain robust (R) stationary state probability density function (PDF) monomodality and preclude metastability is obtained. The PDF transient along deterministic and probability diffusion time scales is characterized, finding that the most probable (MP) state and control as well as their local covariances evolve along nearly deterministic time scale. The compromise between MP state regulation speed, robustness, and control effort is identified, and the stochastic on deterministic dynamics dependency is characterized. The methodological developments and findings are illustrated with three indicative examples with open-loop (OL) complex bimodal and vulcanoid stationary state PDFs.

* Corresponding author

Keywords: Exothermic continuous reactor, PI control, statistical process control, most probable state control, probability density function (PDF) evolution, stochastic nonlinear dynamics, Fokker-Planck partial differential equation.

1. Introduction

Closed-loop (CL) industrial exothermic continuous stirred tank reactors (CSTRs) with complex open-loop (OL) nonlinear (NL) dynamics and linear proportional-integral (PI) control operate in the presence of exogenous (inlet composition and temperature, heat exchange rates, actuator, and measurement, etc.) and endogenous (quasi-stationary dynamics, imperfect mixing-transport, etc.) parasitic (high frequency) fluctuations (Jazwinski, 1970; Risken, 1996; Gardiner, 1997). By complex dynamics it is meant with NL phenomena, that occur "in the large" (beyond locality) such as steady-state (SS) multiplicity and/or limit cycling (LC) (Hubbard and West, 1995). Safety, disturbance and/or fault detection, reliability, product quality assessments and setpoint adjustment (Ratto, 1998; Ratto and Paladino, 2000) are executed in a supervisory layer (Burr, 1976; McAvoy, 2002), by ad hoc combinations of PI and statistical process (SP) control techniques The development of more systematic means to combine PI and SP control is a relevant problem along current industrial trends (Samad, 2017; Maxim et al., 2019).

The OL stochastic stationary dynamics of the indicative 2-state reactor class addressed in the present study has been analyzed over 5 decades mostly with local (per stable SS) Monte Carlo (MC) method-based simulation, reporting that: (i): (i) reasonable state mean and covariance results are obtained in away from deterministic bifurcation condition (Pell and Aris, 1969; Doraiswamy and Kulkarny, 1986; Mandur and Budman, 2014), and (ii) the method breaks down (Pell and Aris, 1969) or yields atypical results (Doraiswamy and Kulkarny, 1986) in close to deterministic bifurcation. Recently (Alvarez et al., 2018), the OL PDF dynamics has been characterized with analytic NL global FP PDE theory (Risken, 1996) that yields rigorous and consistent stationary and transient state PDF results in away from and close to deterministic bifurcation. It was established that: (i) the stationary state PDF is R monomodal if and only if the deterministic global dynamics are R monostable, (ii) there can be or not metastable state PDF evolutions (a purely stochastic phenomenon, inexistent in deterministic systems) [Risken, 1996; Gardiner, 1997], depending on deterministic dynamics characteristics, (iii) a non-metastable state PDF evolves along deterministic and probabilistic time scales, and a metastable one evolves along those two scales as well as along a comparatively slower escape time scale. It was explained why the MC method of previous reactor studies: (i) breaks down in close to deterministic bifurcation, and (ii) cannot describe the purely stochastic phenomena (inexistent in deterministic systems) of transient along diffusion and metastability time scales.

The CL 3-state stochastic stationary dynamics of the above discussed 2-state reactor class with linear PI control has been analyzed local FP theory and MC simulation (Ratto, 1998; Ratto and Paladino, 2000), with emphasis on control gain selection in the light of state mean and variability along SP control considerations. It has been reported that: (i) as in the OL case (Pell and Aris, 1969),

the MC approach breaks down in close to deterministic bifurcation, and (ii) the overcoming of this obstacle for efficient gain tuning requires the global FP PDE approach (Ratto, 1998).

Recently, stochastic exothermic reactors have been stabilized about an OL unstable mean SS with: (i) linear proportional control tuned with a stochastic sensitivity-ellipsoidal confidence technique for a 2-state OL case (Bashkirtseva, 2018; Bashkirtseva and Pisarchik, 2018), and (ii) in a probabilistic sense, stochastic passive NL SF control (Krstic and Deng, 1988; Annunziato et al., 2014) for a 3-state OL case (Lu et al., 2022). In both studies, the multiscale transient response issue was not regarded. In an OL unstable industrial reactor stabilized with P or PI control, a practitioner should be willing to tune such control with a stochastic method in an advisory layer, but skeptical to replace it with a considerably more complex, model dependent, and expensive observer-based deterministic or stochastic NL SF control.

The preceding considerations motivate the present study on the global CL stochastic dynamics of the above discussed class of CL 3-state stochastic exothermic reactors with complex deterministic dynamics and industrial-type linear PI control, and justify its scope and novelty: the FP theory-based formal resolution of the open and longstanding problem (Ratto, 1998; Ratto and Paladino, 2000) of choosing the control gains in the light of SP control considerations, along past current industrial trends (Samad, 2017; Maxim et al., 2019).

The methodological point of the departure is the FP PDE-based PDF modeling of the OL 2-state case (Alvarez et al., 2018), where the correspondence between CL stochastic PDF monomodality and deterministic monostability was established via the analytic solution of the 2-state FP PDE. The resolution of the present CL 3-state reactor problem requires the overcoming of two technical difficulties: (i) the correspondence between CL stochastic PDF monomodality and deterministic monostability must be established with a method that circumvents the difficult or infeasible task analytically solving the CL 3-state stationary state PDF, and (ii) the means to characterize MP state and control evolutions and their variabilities are lacking. These difficulties are overcome by combining notions and tools from: (i) FP PDE fluctuation-dissipation (Ao, 2003; Kwon et al., 2005; Wang et al., 2006) and functional analysis-based dynamics (Jazwinski, 1970; Markowich and Villani, 2000), and (ii) deterministic NL dynamics (La Salle and Lefschetz, 1961; Hirsch and Smale, 1974; Sontag, 2008;) and control (Isidori, 1999).

The contents are organized as follows. In Section 2 the problem is technically stated. In Section 3, the deterministic CL R stability is characterized in terms of passivity and control gains. In Section 4, the correspondence between CL R state PDF monomodality and deterministic monostability is established. In Section 5, the MP state and control and their covariance evolutions are characterized. In Section 6, the proposed approach is illustrated with three examples with OL bimodal and vulcanoid PDFs. In Section 7, conclusions are drawn. The acronyms employed are listed in Table 1.

Table 1. Acronyms

Acronym	Meaning
CL	closed-loop
CSTR	continuous stirred tank reactor
E	exponentially
EU	exponentially ultimately
FV	finite volume
IS	input-to-state
G	geometric
LC	limit cycle
LS	limit set
MP	most probable
NL	nonlinear
ODE	ordinary differential equation
OF	output-feedback
OL	open-loop
P	practically
MC	Monte Carlo
PDE	partial differential equation
PDF	probability density function
PI	proportional-integral
R	robust
SDE	stochastic differential equation
STD	standard deviation
SF	state feedback
SS	steady-state
SP	statistical process
ZD	zero-dynamics

2. Control problem

Consider the class of exothermic CSTRs modeled by the deterministic mass and heat balances in dimensionless form (Aris, 1965; Alvarez et al., 2018):

$$\dot{x}_1 = \theta(x_{1e} - x_1) - \delta r(x_1, x_2) \coloneqq g_1(\boldsymbol{z}, \boldsymbol{d}), \quad \boldsymbol{z}\text{: (3b)} \tag{1a}$$

$$\dot{x}_2 = \theta(x_{2e} - x_2) - \eta(x_2 - \bar{x}_{2c}) + (\delta/2) r(x_1, x_2) + \eta u \coloneqq g_2(\boldsymbol{z}, \boldsymbol{d}, u) \tag{1b}$$

$$y = x_2, \quad x_1(0) = x_{1o}, \quad x_2(0) = x_{2o} \tag{1c}$$

with nominal statics

$$\bar{\theta}(\bar{x}_{1e} - \bar{x}_1) - \delta r(\bar{x}_1, \bar{x}_2) = 0 \tag{2a}$$

$$\bar{\theta}(\bar{x}_{2e} - \bar{x}_2) - \eta(\bar{x}_2 - \bar{x}_{2c}) + (\delta/2) r(\bar{x}_1, \bar{x}_2) = 0 \tag{2b}$$

where

$$x_1 = C/C_r, \qquad x_1 = T/T_r, \qquad u = x_{2c} - \bar{x}_{2c}$$

$$C_r = \bar{C}_e, \qquad T_r = \bar{T}_e, \qquad T_a = (-\Delta_a) C_r/(\rho c_p T_r), \quad \eta = UA/(\bar{Q}\rho c_p) >_r 0$$

$$\theta = Q/\bar{Q}, \qquad (\dot{\cdot}) = \frac{d(\cdot)}{dt}, \qquad t = t_a/t_\theta\,, \qquad t_\theta = V/\bar{Q},$$

$$\delta = \bar{R}V/(\bar{Q}\, C_r, \qquad r(x_1, x_2) = R(C_r x_1, T_r x_2)/\bar{R}, \qquad \bar{R} = R(\bar{C}, \bar{T})$$

In the ODE (1): x_1 (or x_2) is the concentration (or temperature) state, x_{1e} (or x_{2e}) is the feed concentration (or temperature) input, x_{2c} is the coolant temperature, δ (or η) is the Damköhler (or Stanton) dimensionless number, r is the reaction rate function, t_θ (or θ) is the dimensionless nominal residence time (or dilution rate), y is the measured temperature, u is the jacket temperature control in deviation form with respect to the setpoint $\bar{y}$ associated with the (possibly nonunique and unstable) stable steady-state (SS) concentration-temperature pair $(\bar{x}_1, \bar{x}_2)$ of the nominal statics (2).

2.1 Open-loop (OL) deterministic dynamics

In vector form, the *deterministic nonlinear (NL) OL 2-state reactor dynamics* (1) are written as

$$\dot{\boldsymbol{z}} = \boldsymbol{g}(\boldsymbol{z}, \boldsymbol{d}, u), \quad \boldsymbol{z}(\boldsymbol{0}) = \boldsymbol{z}_o, \quad y = \boldsymbol{c}_z \boldsymbol{z}, \; t \geq 0, \quad \boldsymbol{z} \in Z \subset \Re^2, \quad \boldsymbol{d} \in D \subset \Re^2 \tag{3a}$$

where

$$\boldsymbol{z} = (x_1, x_2)^T, \qquad \boldsymbol{g} = (g_1, g_2)^T, \quad \boldsymbol{c}_z = (0,1), \quad g_1, g_2\text{: (1a-b)}, \qquad \boldsymbol{d} = (\theta, x_{1e}, x_{2e})^T \tag{3b}$$

$$Z = \{\boldsymbol{z} = (x_1, x_2)^T \in \Re^2 | 0 \leq x_1 \leq x_1^+, x_2^- \leq x_2 \leq x_2^+\} \tag{3c}$$

$$x_1^+ = x_{1e}^+, \qquad x_2^- = \frac{\bar{\theta} x_{2e}^- + \eta x_{2c}^-}{\bar{\theta} + \eta}, \qquad x_2^+ = \frac{(\delta/2) + \bar{\theta} x_{2e}^+ + \eta x_{2c}^+}{\bar{\theta} + \eta} \tag{3d}$$

$\boldsymbol{z}$ (or $\boldsymbol{d}$) is the *state* (or input disturbance) in the bounded set Z (or D), Z is the invariant state space (Alvarez et al., 2018), and $\boldsymbol{z}_o$ is the initial state. The corresponding *limit set* (LS) is

$$\mathfrak{S}_z = \mathcal{S}_z \cup \mathcal{L}_z \tag{4a}$$

where

$$\mathcal{S}_z = \{\bar{\boldsymbol{z}}_1, \dots, \bar{\boldsymbol{z}}_{n_s \geq 1}\} \supset \mathcal{S}_z^s, \qquad \boldsymbol{g}(\bar{\boldsymbol{z}}_i, \bar{\boldsymbol{d}}, 0) = 0, \quad \bar{\boldsymbol{z}} \in \mathcal{S}_z \tag{4b}$$

is the set of steady-states (SSs), and

$$\mathcal{L}_z = \{\bar{\boldsymbol{z}}_1(t), \dots, \bar{\boldsymbol{z}}_{n_l}(t)\}, \qquad \boldsymbol{g}[\bar{\boldsymbol{z}}_i(t), \bar{\boldsymbol{d}}, 0] = \dot{\boldsymbol{z}}_i(t) \tag{4c}$$

is the set of limit cycles (LCs), $\mathcal{S}_z^s$ is the set of stable SSs, and $\bar{\boldsymbol{z}}$ is the prescribed SS.

When the reaction rate r in (3) is 1st-order (linear) in concentration and NL (with Arrhenius dependency) in temperature, over its Damköhler-Stanton (δ-η) parameter space the deterministic reactor (3) has regions of monostability, bistability and limit cycling, delimited by saddle-node and Hopf bifurcation (Aris, 1965; Uppal et al., 1974; Aris, 1999; Alvarez et al., 2018).

For given $[\boldsymbol{z}_o, (\boldsymbol{d}, u)(t)]$, the OL NL ODE (3) has a unique solution *state* motion

$$\boldsymbol{z}(t) = \boldsymbol{\tau}_{\boldsymbol{z}}[t, \boldsymbol{z}_o, (\boldsymbol{d}, u)(t)] \tag{5a}$$

and *measured output signal*

$$y(t) = \boldsymbol{c}_z\{\boldsymbol{\tau}_{\boldsymbol{z}}[t, \boldsymbol{z}_o, (\boldsymbol{d}, u)(t)]\} \tag{5b}$$

When $(\boldsymbol{d}, u) = (\bar{\boldsymbol{d}}, 0)$, and $\boldsymbol{z}_o$ is not a stable SS, $\boldsymbol{z}(t)$ reaches asymptotically, with characteristic time t_z, a SS $\bar{\boldsymbol{z}}$ or a LC $\bar{\boldsymbol{z}}(t)$ (Gavalas, 1968; Alvarez et al., 1991), i.e.,

$$(\boldsymbol{d}, u)(t) = (\bar{\boldsymbol{d}}, \bar{u}), \quad \boldsymbol{z}_o \notin \mathcal{S}_z^s \;\; \Rightarrow \;\; \boldsymbol{z}(t) \overset{t_z}{\to} \bar{\boldsymbol{z}} \in \mathcal{S}_z \;\; \text{or} \;\; \bar{\boldsymbol{z}}(t) \in \mathcal{L}_z, \quad t_z = 1/\lambda_z \tag{6}$$

2.2 Open-loop (OL) stochastic dynamics

The effect in the deterministic dynamics (3) of parasitic fluctuations (flow, temperature, and concentration variations, as well as reaction and mixing-transport quasi-SS assumptions) is expressed as a zero-mean uncorrelated white noise exogenous concentration (ξ_1) and temperature (ξ_2) rate of change inputs, according to the stochastic differential equations (SDEs) (Pell and Aris, 1969; Doraiswamy and Kulkarni, 1986; Ratto, 1998; Alvarez et al., 2018):

$\dot{z}_1 = g_1(z_1, z_2, \theta, x_{1e}) + \xi_1(t), \quad z_1(0) = z_{1o}, \quad \xi_1(t) = \mathcal{W}(0, q_1), \quad g_1, g_2$: (1a-b) (7a)

$\dot{z}_2 = g_2(z_1, z_2, \theta, x_{2e}, u) + \xi_2(t), \quad z_2(0) = z_{2o}, \quad \xi_2(t) = \mathcal{W}(0, q_2), \quad y = z_2$ (7b)

which in vector form are written as the [also called Langevin (Risken, 1996)] equation

$\dot{\boldsymbol{z}} = \boldsymbol{g}(\boldsymbol{z}, \boldsymbol{d}, u) + \boldsymbol{\xi}(t), \quad \boldsymbol{z}(0) = \boldsymbol{z}_o \sim \mathcal{R}[\varsigma_o(\boldsymbol{z})], \quad y = \boldsymbol{c}_z(\boldsymbol{z}), \quad \boldsymbol{z} \in \mathcal{Z} \supseteq Z$ (8a)

where

$\boldsymbol{\xi}(t) = \mathcal{W}[\boldsymbol{0}, \boldsymbol{Q}], \qquad \boldsymbol{\xi} = (\xi_1, \xi_2)^T, \qquad \boldsymbol{Q} = \begin{bmatrix} q_1 & 0 \\ 0 & q_2 \end{bmatrix}, \qquad q_1, q_2 > 0$ (8b-d)

$\mathcal{Z} = \{\boldsymbol{z} \in \Re^2 | 0 \le x_1 \le (1+\varepsilon_1)x_1^+, (1-\varepsilon_2)x_2^- \le x_2 \le (1+\varepsilon_2)x_2^+\}, \quad x_1^+, x_2^-, x_2^+$: (3d), $\varepsilon_i \approx \frac{1}{3}$ (8e)

$\boldsymbol{z}_o$ is the initial random state $\boldsymbol{z}_o$ with probability density function (PDF) $\varsigma_o(\boldsymbol{z})$ over the probabilistic state space $\mathcal{Z}$ (Alvarez et al., 2018).

For given $[\varsigma_o, (\boldsymbol{d}, u)(t), \boldsymbol{Q}]$, the SDE (8) has as unique solution a bivariate *state PDF motion* (Risken, 1996; Gardiner, 1997)

$\varsigma(\boldsymbol{z}, t) = \tau_\varsigma[t, \varsigma_o(\boldsymbol{z}), \boldsymbol{d}(t), u(t)], \qquad \varsigma(\boldsymbol{z}, t) \ge 0$ (9)

that: (i) satisfies the 2-state dynamic FP PDE (10) [presented and discussed in (Alvarez et al., 2018)]

$t > 0, \boldsymbol{z} \in \mathcal{I}_{\mathcal{Z}}$: $\quad \partial_t \varsigma = \boldsymbol{\nabla} \cdot \left[\frac{1}{2}\boldsymbol{Q}\boldsymbol{\nabla}\varsigma - \boldsymbol{g}(\boldsymbol{z}, \boldsymbol{d})\varsigma\right]$ (10a)

$t = 0, \boldsymbol{z} \in \mathcal{Z}$: $\quad \varsigma(\boldsymbol{z}, 0) = \varsigma_o(\boldsymbol{z}); \quad t \ge 0$: $\int_{\mathcal{Z}} \varsigma(\boldsymbol{z}, t) d\boldsymbol{z} = 1$ (10-c)

$t \ge 0, \boldsymbol{z} \in \mathcal{B}_{\mathcal{Z}}$: $\quad \frac{1}{2}\boldsymbol{Q}\boldsymbol{\nabla}\varsigma - \boldsymbol{g}(\boldsymbol{z}, \boldsymbol{d})\varsigma = \boldsymbol{0}$ (10d)

and (ii) when $(\boldsymbol{d}, u) = (\bar{\boldsymbol{d}}, 0)$ and $\varsigma_o(\boldsymbol{z}) \ne \bar{\varsigma}(\boldsymbol{z})$, $\varsigma(\boldsymbol{z}, t)$ (9) reaches asymptotically (along time scale t_ς with deterministic, diffusion and escape time subscales), a stationary state PDF

$\bar{\varsigma}(\boldsymbol{z}) \ge 0, \qquad \int_{\mathcal{Z}} \bar{\varsigma}(\boldsymbol{z}) d\boldsymbol{z} = 1, \quad \boldsymbol{z} \in \mathcal{Z} \supseteq Z$ (11a)

according to the expressions

$\boldsymbol{d} = \bar{\boldsymbol{d}}, \quad u = 0, \quad \varsigma_o(\boldsymbol{z}) \ne \bar{\varsigma}(\boldsymbol{z}) \quad \Rightarrow \quad \varsigma(\boldsymbol{z}, t) \overset{t_\varsigma}{\to} \bar{\varsigma}(\boldsymbol{z})$, (11b)

where

$t_\varsigma \approx \begin{cases} t_e^o \ge t_d^o & \text{if } \varsigma(\boldsymbol{z}, t) \text{ is metastable} \\ t_d^o \ge t_z & \text{if } \varsigma(\boldsymbol{z}, t) \text{ is not metasable} \end{cases}, \quad t_d^o \approx 1/\min(q_1, q_2) > t_z, \quad t_z = 1/\lambda_z$ (11c)

$\mathcal{E}_z = \mathfrak{S}_z \ni \bar{\boldsymbol{z}}, \quad \bar{y} = \boldsymbol{c}_z(\bar{\boldsymbol{z}}), \quad \mathfrak{S}_z$: (4) (11d)

t_z, t_d^o, and t_e^o are the OL deterministic diffusion and escape time scales, respectively, $\mathcal{E}_z$ -equal to the deterministic LS (4)- is the *extremum set (ES)* of $\bar{\varsigma}(\boldsymbol{z})$, and $\bar{\boldsymbol{z}}$ is the OL (possibly a minimum or saddle)

extremum point of interest, which determines the temperature setpoint $\bar{y}$ for the CL reactor SDE with PI control that will be discussed in the next two subsections.

When the reaction rate r in (3) is linear (or NL with Arrhenius dependency) in concentration (or temperature), over its Damköhler-Stanton (δ-η) parameter space the stationary state PDF $\bar{\varsigma}(\boldsymbol{z})$ (11a) has regions of monomodality, bimodality, and vulcanoid shape underlain by deterministic monostability, bistability and limit cycling, respectively (Alvarez et al., 2018).

As mentioned in the introduction (Alvarez et al., 2018): (i) the OL PDF responses $\varsigma(\boldsymbol{z}, t)$ (9) along diffusion (t_d^o) and metastability (t_e^o) scales are purely stochastic phenomena (inexistent in deterministic systems) that are captured by the underlying FP PDE, and not by the local (Doraiswamy and Kulkarni, 1986; Ratto, 1998; Ratto and Paladino, 2000) and global (Vesterinen and Ritala, 2005) ODE simulation-based MC methods employed in previous OL and CL chemical reactor studies, and (ii) PDF motion (9) metastability (11c) is a per-state PDF motion property (and not a per-system generic one), which is generically ruled out by stationary state PD monomodality. Thus, attainment of CL robust PDF monomodality is a fundamental control task, especially when the OL PDF is not R monomodal.

2.3 Closed-loop PDF dynamics

Consider the industrial-type *deterministic linear PI control*

$$u = PI(y), \qquad PI(y) := \bar{u} - k_p\{(y - \bar{y}) + \tau_I^{-1}\int_0^t [y(t) - \bar{y}]dt\} \tag{12a}$$

with proportional gain k_p, reset time τ_I, integral gain k_I, set point

$$\bar{y} = \boldsymbol{c}_z\bar{\boldsymbol{z}} \in S_z \ni \boldsymbol{g}(\bar{\boldsymbol{z}}, \bar{\boldsymbol{d}}) = \boldsymbol{0}, \quad \boldsymbol{g}\text{: (1a-b)} \tag{12b}$$

determined by the nominal target (possibly, neither unique nor maximum) extremum $\bar{\boldsymbol{z}}$ (4) of the bivariate OL PDF (11a), and gain set

$$K = \{\boldsymbol{k} \in \Re^2 | 0 < k_p \le k_p^+, 0 < k_I \le k_I^+\}, \quad \boldsymbol{k} = [k_p, k_I]^T, \quad k_I = k_p/\tau_I \tag{12c}$$

In the presence of measurement (or actuator) zero-mean uncorrelated white noise error w_y (or ξ_u) with variance q_y (or q_u), the measurement (y) and control (u) become random variables, and the PI controller (12a) acquires the *random variable form*

$$u = PI(y + w_y) + \xi_u, \qquad \xi_u = \mathcal{W}(0, q_u), \qquad w_y = \mathcal{W}(0, q_y) \tag{13a-c}$$

The application of this control to the OL NL 2-state SDE (8) yields the *CL NL 3-state SDE*

$$\dot{x}_1 = f_1(x_1, x_2, \theta, x_{1e}) + w_1, \qquad x_1(0) = x_{1o} \tag{14a}$$

$$\dot{x}_2 = f_2(x_1, x_2, x_3, \theta, x_{2e}, k_p) + w_2, \qquad x_2(0) = x_{2o} \tag{14b}$$

$$\dot{x}_3 = f_3(x_2, k_I) + w_3, \qquad x_3(0) = x_{3o} \tag{14c}$$

$$y = \boldsymbol{c}_y\boldsymbol{x} - k_p w_y, \quad u = \boldsymbol{c}_u\boldsymbol{x} + w_u \tag{14d}$$

where

$$f_1(x_1, x_2, \theta, x_{1e}) = g_1(x_1, x_2, \theta, x_{1e}), \qquad f_3(x_2, k_I) = k_I(x_2 - \bar{x}_2) \tag{14e}$$

$$f_2(x_1, x_2, x_3, \theta, x_{2e}, k_p) = g_2(x_1, x_2, x_3, \theta, x_{2e}) - \eta[k_p(x_2 - \bar{x}_2) + x_3] \quad (14f)$$

$$\boldsymbol{c}_y = (0\ 1\ 0), \quad \boldsymbol{c}_u = \eta[0\ k_p\ 1], \quad g_1, g_2\text{: (1a-b)} \quad (14g)$$

$$\boldsymbol{w} = \begin{bmatrix} w_1 \\ w_2 \\ w_3 \end{bmatrix} = \mathcal{W}[\boldsymbol{0}, \boldsymbol{Q}(\boldsymbol{k})], \qquad \boldsymbol{Q}(\boldsymbol{k}) = \begin{bmatrix} q_1 & 0 & 0 \\ 0 & q_2(k_p) & q_c(\boldsymbol{k}) \\ 0 & q_c(\boldsymbol{k}) & q_3(k_I) \end{bmatrix} \quad (14h)$$

and $\boldsymbol{w}$ is a CL zero-mean correlated white noise vector with gain dependent covariance 3x3 matrix $\boldsymbol{Q}$ is the gain-dependent covariance matrix of the with entries

$$q_1 = q_{\theta 1}, \quad q_2(k_p) = q_{\theta 2} + \eta^2(q_{\theta u} + k_p^2 q_y), \quad q_3(k_I) = k_I^2 q_y, \quad q_c(\boldsymbol{k}) = -\eta k_p k_I q_y \quad (14j)$$

In compact vector form, the CL 3-state SDE (14) is written as

$$\dot{\boldsymbol{x}} = \boldsymbol{f}(\boldsymbol{x}, \boldsymbol{d}, \boldsymbol{k}) + \boldsymbol{w}, \quad \boldsymbol{x}_o = \mathcal{R}[\pi_o(\boldsymbol{x})] \quad (15a)$$

$$y = \boldsymbol{c}_y \boldsymbol{x} + w_y, \quad u = \boldsymbol{c}_u \boldsymbol{x} + w_u, \quad \boldsymbol{x} \in \mathcal{X}, \quad u \in \mathcal{U}, \quad \boldsymbol{k} \in K \quad (15b)$$

where

$$\boldsymbol{x} = [x_1\ x_2\ x_3]^T, \quad \boldsymbol{f} = [f_1\ f_2\ f_3]^T, \quad \boldsymbol{w}\text{: (14h)}, \quad \mathcal{X} = \mathcal{Z} \times \mathcal{I} \supseteq X, \quad \mathcal{Z}\text{: (8e)} \quad (15c)$$

$$\mathcal{I} = \{x_3 \in \Re | (1 - \varepsilon_3)x_3^- \le x_3 \le (1 + \varepsilon_2)x_3^+\}, \quad \varepsilon_3 \approx 1/3 \quad (15d)$$

$$f_1, f_2, f_3\text{: (14e-f)}, \quad \boldsymbol{c}_y, \boldsymbol{c}_u\text{: (14g)}, \quad K\text{: (12c)}$$

For given $[\pi_o(\boldsymbol{x}), \boldsymbol{d}(t), \boldsymbol{Q}(\boldsymbol{k})]$, the SDE (15) has as unique *state PDF motion solution* (Risken, 1996; Gardiner, 1997)

$$\pi(\boldsymbol{x}, t) = \tau_\pi[t, \pi_o(\boldsymbol{x}), \boldsymbol{d}(t), \boldsymbol{k}], \quad \pi(\boldsymbol{x}, t) \ge 0 \quad (16)$$

that satisfies the dynamic 3-state FP PDE with initial (17b), conservation (17c) and boundary (17d) conditions:

$$t > 0, \boldsymbol{x} \in \mathcal{I}_\mathcal{X}\text{:} \qquad \partial_t \pi = \boldsymbol{\nabla} \cdot \left[\tfrac{1}{2}\boldsymbol{Q}\boldsymbol{\nabla}\pi - \boldsymbol{f}(\boldsymbol{x}, \boldsymbol{d})\pi\right] := \mathcal{F}(\pi, \boldsymbol{d}, \boldsymbol{k}) \quad (17a)$$

$$t = 0, \boldsymbol{x} \in \mathcal{X}\text{:} \qquad \pi(\boldsymbol{x}, 0) = \pi_o(\boldsymbol{x}); \qquad t \ge 0\text{: } \int_\mathcal{X} \pi(\boldsymbol{x}, t) d\boldsymbol{x} = 1 \quad (17b\text{-}c)$$

$$t \ge 0, \boldsymbol{x} \in \mathcal{B}_\mathcal{X}\text{:} \qquad \tfrac{1}{2}\boldsymbol{Q}\boldsymbol{\nabla}\pi - \boldsymbol{f}(\boldsymbol{x}, \boldsymbol{d})\pi := \boldsymbol{\mathcal{B}}(\pi, \boldsymbol{d}, \boldsymbol{k}) = \boldsymbol{0} \quad (17d)$$

$$t \ge 0,\ u \in \mathcal{U}\text{:} \qquad \nu(u, t) = h[\pi(\boldsymbol{x}, t)] \ge 0, u \in \mathcal{U} \quad \int_\mathcal{U} \nu(u, t) du = 1 \quad (17e)$$

$$t \ge 0, \boldsymbol{x} \in \mathcal{X}\text{:} \qquad \boldsymbol{\psi} = \mathcal{Y}[\pi(\boldsymbol{x}, t)] \quad (17f)$$

$\mathcal{X}$ is the probabilistic state space with interior (or boundary) $\mathcal{I}_\mathcal{X}$ (or $\mathcal{B}_\mathcal{X}$), and the output

$$\boldsymbol{\psi} = \{\boldsymbol{\psi}_1, \boldsymbol{\psi}_2\}, \quad \boldsymbol{\psi}_1 = \{\boldsymbol{x}_m, u_m, \Sigma_m, \sigma_u\} \quad (18a)$$

contains the PDF properties of interest in industrial statistical process control.

In the output $\boldsymbol{\psi}_1$ (18a) are included: (i) the state ($\boldsymbol{x}_m$) control (u_m) PDF modes (most probable values)

$$\boldsymbol{x}_m(t) = \arg\max_{\pi \in \mathcal{X}} \pi(\boldsymbol{x}, t) := \boldsymbol{m}_x[\pi(\boldsymbol{x}, t)], \qquad \boldsymbol{\nabla}\pi(\boldsymbol{x}_m, t) = \boldsymbol{0} \quad (18b)$$

$$u_m(t) = \arg\max_{u \in \mathcal{U}} \nu(u, t) := m_u[\nu(u, t)], \qquad \partial_u \nu(u_m, t) = 0 \quad (18c)$$

and (ii) the corresponding state (Σ_m) and control (σ_u) variabilities (covariances)

$$\Sigma_m[\pi(\boldsymbol{x}, t)] = \boldsymbol{H}^{-1}(\boldsymbol{x}_m, t), \quad \sigma_u = \boldsymbol{v}_u(\operatorname{diag}\boldsymbol{\Sigma}_m)\boldsymbol{v}_u^T, \quad \boldsymbol{v}_u = (0, k_p, 1) \quad (18d)$$

where

$$\boldsymbol{H}(\boldsymbol{x},t)=\boldsymbol{\mathcal{H}}\pi(\boldsymbol{x},t),\qquad \boldsymbol{\mathcal{H}}=\boldsymbol{\nabla}\boldsymbol{\nabla}^T,\quad \boldsymbol{\nabla}=(\partial_{x_1},\partial_{x_2},\partial_{\partial_{x_3}})^T \tag{18e}$$

$$\nu(u,t)=\frac{1}{k_p}\int_{x_3^-}^{x_3^+}\mu_{x_2}[(u-x_3)/k_p]\mu_{x_3}(x_3,t)dx_3 \tag{18f}$$

$$\mu_{x_i}(x_i,t)=\int_{x_k^-}^{x_k^-}\int_{x_j^-}^{x_j^+}\pi(\boldsymbol{x},t)dx_jdx_k,\ \ i=1,2,3,\quad j,k\neq i \tag{18g}$$

$\boldsymbol{\nabla}$ (or $\boldsymbol{\mathcal{H}}$) is the gradient vector (or matrix Hessian) operator, (18e) determines the 1D control PDF ν from the 3D state one π (Papoulis and Pillai, 2002), and μ_{x_i} is the marginal PDF with respect to the state x_i (Papoulis and Pillai, 2002). In the output $\boldsymbol{\psi}_2$ (18a) can be included other properties such as state and control mean and their variabilities, as well as skewness measures like kurtocity.

When $\boldsymbol{d}=\bar{\boldsymbol{d}}$ and $\pi_o(\boldsymbol{x})\neq\bar{\pi}(\boldsymbol{x})$, the PDF motion state motion $\pi(\boldsymbol{x},t)$ (16) and control evolution $\nu(u,t)$ (18f) reach asymptotically (along time scale t_π) the stationary PDFs $\bar{\pi}(\boldsymbol{x})$ and $\bar{\nu}(u)$, i.e.,

$$\boldsymbol{d}=\bar{\boldsymbol{d}},\ \ \pi_o(\boldsymbol{x})\neq\bar{\pi}(\boldsymbol{x})\ \ \Rightarrow\ \ \pi(\boldsymbol{x},t)\overset{t_\pi}{\to}\bar{\pi}(\boldsymbol{x}),\quad \nu(u,t)\overset{t_\pi}{\to}\bar{\nu}(u),\quad \boldsymbol{\psi}\overset{t_\pi}{\to}\bar{\boldsymbol{\psi}}(u) \tag{19a}$$

where

$$t_\pi(\boldsymbol{k})\approx\begin{cases}t_e\geq t_d & \text{if } \pi(\boldsymbol{x},t) \text{ is metastable}\\ t_d\geq t_x & \text{if } \pi(\boldsymbol{x},t) \text{ is not metastable}\end{cases},\quad t_d\approx 1/\min(q_1,q_2,q_3)>t_x=1/\lambda_x \tag{19b}$$

t_x, t_d, and t_e are the CL deterministic, diffusion, and escape time scales, respectively, with stationary state PDF

$$\bar{\pi}(\boldsymbol{x})\geq 0,\ \ \int_{\mathcal{X}}\bar{\pi}(\boldsymbol{x})d\boldsymbol{x}=1;\quad \bar{\nu}(u)\geq 0,\ \ \int_{\mathcal{U}}\bar{\nu}(u)du=1 \tag{20}$$

The stationary state PDF (20): (i) uniquely satisfies the static FP PDE

$$\boldsymbol{x}\in\mathcal{I}_{\mathcal{X}}:\ \ \mathcal{F}(\bar{\pi},\bar{\boldsymbol{d}})=0,\ \ \int_{\mathcal{X}}\pi(\bar{\pi},t)d\boldsymbol{x}=1 \tag{21a}$$

$$\boldsymbol{x}\in\mathcal{B}_{\mathcal{X}}:\ \boldsymbol{\mathcal{B}}(\bar{\pi},\bar{\boldsymbol{d}})=\boldsymbol{0} \tag{21b}$$

$$u\in\mathcal{U}:\ \ \bar{\nu}=h(\bar{\pi})\geq 0,\ u\in\mathcal{U},\quad \int_{\mathcal{U}}\nu(u,t)du=1 \tag{21c}$$

$$\boldsymbol{x}\in\mathcal{X}:\ \ \bar{\boldsymbol{\psi}}=\mathcal{Y}(\bar{\pi}) \tag{21d}$$

and (ii) has the extremum set (ES)

$$\mathcal{E}=\mathcal{P}\cup\mathcal{O},\ \mathcal{P}=\{\boldsymbol{x}_1,\dots,\boldsymbol{x}_{n_{p\geq 1}}\},\quad \boldsymbol{\nabla}\bar{\pi}(\boldsymbol{x}_i,\boldsymbol{k})=\boldsymbol{0} \tag{21a}$$

where

$$\mathcal{P}=\{\boldsymbol{x}_1,\dots,\boldsymbol{x}_{n_{p\geq 1}}\},\qquad \boldsymbol{\nabla}\bar{\pi}(\boldsymbol{x}_i,\boldsymbol{k})=\boldsymbol{0} \tag{21a}$$

is the set of extremum points $\boldsymbol{x}_i$, and

$$\mathcal{O}=\{\mathcal{O}_1,\dots,\mathcal{O}_{n_{c\geq 0}}\},\quad \mathcal{O}_i=\{\boldsymbol{x}\in\mathcal{X}|[\boldsymbol{\nabla}\bar{\pi}(\boldsymbol{x})]\cdot\boldsymbol{n}_i(\boldsymbol{x})\}=0,\ \ \bar{\boldsymbol{x}}_m=\boldsymbol{m}_x(\bar{\pi}),\ \boldsymbol{m}_x\text{: (18b)} \tag{21b}$$

is the set of extremum curves $\mathcal{O}_i$ with normal unit vector $\boldsymbol{n}_i(\boldsymbol{x})$.

A CL stationary monomodal PDF with prescribed mode $\bar{\boldsymbol{x}}_m=\bar{\boldsymbol{x}}$ is called $\bar{\boldsymbol{x}}_m$-monomodal, and the set of gain pairs that yield $\bar{\boldsymbol{x}}_m$-monomodality is denoted by

$$K_m=\{\boldsymbol{k}\in K|\mathcal{E}=_r\bar{\boldsymbol{x}}_m=\bar{\boldsymbol{x}}\},\qquad \bar{\boldsymbol{x}}=(\bar{\boldsymbol{z}}^T,0)^T \tag{22}$$

2.4 Problem

Our problem and contribution consist in characterizing, on the basis of the FP PDE (17) and as improvement of the ones presented in Ratto's pioneering study (Ratto, 1998), the PI control gain pair conditions (22) so that:

(i) The CL state PDF is R $\overline{\boldsymbol{x}}_m$-monostable with mode $\overline{\boldsymbol{x}}_m = \overline{\boldsymbol{x}}$ (implying preclusion of metastability) at prescribed value $\overline{\boldsymbol{x}}$ associated to the nominal OL deterministic (possibly unstable) SS $\overline{\boldsymbol{z}}$ (4b).

(ii) MP state (18b) regulation as close as possible to deterministic time scale with admissible state and control mode (18b) and their variabilities.

Methodologically, we are interested in characterizing:

(i) The state [$\pi(\boldsymbol{x}, t)$: (17a-d)] control [$\nu(u, t)$: (18f)] PDF evolutions along deterministic and probabilistic diffusion time scales.

(ii) The compromise between regulation capability of PDF characteristics of interest, robustness, and MP control effort measured by MP state u_m and its variability.

(iii) The stochastic on deterministic dynamics dependency, to enable the exploitation the valuable accumulated knowledge on the complex nonlinear dynamics of the deterministic exothermic reactor class (Aris, 1965; Uppal et al., 1974).

The preceding specific and methodological problem are solved by combining notions and tools from: (i) the stochastic fluctuation-dissipation relationship associated to the FP PDE (Ao, 2003; Kwon et al., 2005; Wang et al., 2006), (ii) functional analysis-based FP PDE characterization (Jazwinski, 1970, Markowich and Villani, 2000; Frank, 2006), and (iii) deterministic NL dynamics (La Salle and Lefschetz, 1961; Hirsch and Smale, 1974; Hubbard and West, 1995; Sontag, 2008) and passive control (Hirschorn, 1979; Isidori, 1999; Khalil, 2002; Sontag, 2008).

It must be pointed out that, while in a previous study (Alvarez et al., 2018) on the OL 2-state reactor class (8) the correspondence between PDF monomodality and deterministic monostability was established with the analytic solution for the stationary FP PDE (11), here the same correspondence for the 3-state CL stochastic reactor (15a) is obtained without having to solve analytically the 3D FP PDE (17).

To simply the notation, the explicit dependencies of vector, matrices, and operators on the gain $\boldsymbol{k}$ will be omitted and written explicity when convenient.

3. Closed-loop deterministic dynamics

As a fundamental ingredient for the CL stochastic dynamics assessment problem at hand, here the deterministic CL dynamics are characterized.

The elimination of noise in the SDE (15) yields the CL deterministic dynamics

$$\dot{\boldsymbol{x}} = \boldsymbol{f}(\boldsymbol{x}, \boldsymbol{d}), \quad \boldsymbol{x}(0) = \boldsymbol{x}_o, \quad \boldsymbol{x} \in X, \ \boldsymbol{f}\text{: (14e-f)} \tag{23a}$$

$$y = \boldsymbol{c}_y \boldsymbol{x}, \quad u = \boldsymbol{c}_u(\boldsymbol{x}), \quad u \in U, \ \boldsymbol{c}_y, \boldsymbol{c}_u\text{: (14g)}, \ \boldsymbol{k} \in K\text{: (12c)} \tag{23b}$$

with: (i) compact invariant set

$X = Z \times I$, Z: (3c), $I = \{x_3 \in \Re | (x_3^- \leq x_3 \leq x_3^+\}$ (23c)

(ii) statics

$\boldsymbol{f}(\overline{\boldsymbol{x}}, \overline{\boldsymbol{d}}) = \boldsymbol{0}$, $\bar{y} = \boldsymbol{c}_y \overline{\boldsymbol{x}} = \boldsymbol{c}_z \overline{\boldsymbol{z}} \in S_z$, $\bar{u} = 0$ (24)

(iii) state motion

$\boldsymbol{x}(t) = \tau_{\boldsymbol{x}}[t, \boldsymbol{x}_o, \boldsymbol{d}(t)]$, $y(t) = \boldsymbol{c}_y\{\tau_{\boldsymbol{x}}[t, \boldsymbol{x}_o, \boldsymbol{d}(t)]\}$ (25)

and (iv) limit set

$\mathfrak{S}_x = \mathcal{S}_x \cup \mathcal{L}_x$ (26a)

where

$\mathcal{S}_x = \{\overline{\boldsymbol{x}}_1, \dots, \overline{\boldsymbol{x}}_{n_s \geq 1}\} \ni \overline{\boldsymbol{x}}$, $\boldsymbol{f}(\overline{\boldsymbol{x}}_i, \overline{\boldsymbol{d}}) = 0$, $\overline{\boldsymbol{x}} = (\overline{\boldsymbol{z}}^T, \bar{x}_3)^T$, $\bar{x}_3 = 0$, $\overline{\boldsymbol{z}}$: (4b) (26b)

is the set of SS points $\overline{\boldsymbol{x}}_1$, and

$\mathcal{L}_x = \{O_1(t), \dots, O_{n_l}(t)\}$, $\boldsymbol{f}[\overline{\boldsymbol{x}}_i(t), \overline{\boldsymbol{d}}] = \dot{\boldsymbol{z}}_i(t)$, $O_i = \{\boldsymbol{x} \in X | \boldsymbol{x} = \overline{\boldsymbol{x}}_i(t), 0 \leq t \leq t_i^x\}$ (26c)

is the set of SS limit cycles (LCs) points $\overline{\boldsymbol{x}}_i(t)$. A central aim of this section is the characterization of the gain set K_m (22) where the CL is R $\overline{\boldsymbol{x}}$-monostable (at the prescribed SS $\overline{\boldsymbol{x}}$).

3.1 Passivity

Following the NL SF control approach (Isidori, 1999; Sepulchre et al., 2012) for chemical reactors (Alvarez et al., 1991), the enforcement of the setpoint ($\bar{y}$)-based isothermal operation conditions

$x_2 = \bar{y} = \bar{x}_2$, $\dot{x}_2 = 0$ (27)

on the OL deterministic reactor (3) yields the 1-dimensional dynamical inverse (Hirschorn, 1979)

$\dot{x}_1 = g_z(x_1, \bar{y}, \theta, x_{1e})$, $x_1(0) = x_{1o}$; $u = \mu_z(x_1, \theta, x_{2e})$, $x_1 \in X_1 = [0, \bar{x}_{1e}^+]$ (28a-b)

where

$g_z(x_1, \bar{y}, \theta, x_{1e}) = \theta(x_{1e} - x_1) - \delta r(x_1, \bar{y})$, $g_z(\bar{x}_1, \bar{y}, \bar{\theta}, \bar{x}_{1e}) = 0$ (28c-d)

$\mu_z(x_1, \theta, x_{2e}) = -\frac{1}{\eta}[\theta(x_{2e} - \bar{y}) - \eta(\bar{y} - \bar{x}_{2c}) + (\delta/2) r(x_1, \bar{y})]$, $\eta \neq_r 0$ (28e-f)

(28a) is the isothermal (at temperature $x_2 = \bar{y}$) concentration zero (output deviation) (ZD) dynamics (1a), (28b) is the output map that adjusts the control u to keep the temperature fixed at $\bar{x}_2$, and $\eta \neq_r 0$ is the associated relative degree equal to one (RD = 1) condition. The OL reactor (3) is passive if: (i) it has RD = 1 (28e), and (ii) its ZD (28a) are R $\bar{x}_1$-monostable.

The RD = 1 condition is met with a sufficiently large Stanton number $\eta >_r 0$. The ZD (28a) are R $\bar{x}_1$-monostable if and only if the map g_z (28c): (i) is R x_1-antitonic over X_1, i.e.,

$\partial_{x_1} f_1(x_1, \bar{y}, \theta, x_{1e}) = -\theta - \partial_{x_1} r(x_1, \bar{y}) <_r 0 \; \forall \; x_1 \in X_1$ (29a)

and (ii) with $(\bar{\theta}, \bar{x}_{1e})$, it vanishes at the nominal concentration value $\bar{x}_1$, i.e.,

$g_z(\bar{x}_1, \bar{y}, \bar{\theta}, \bar{x}_{1e}) = 0$ (29b)

This passivity characterization is summarized in the next proposition.

Proposition 1. The deterministic OL system (3) is R passive if and only if

(i) $\eta \neq_r 0$, (ii) $\bar{\theta} + \partial_{x_1} r(x_1, \bar{y}) >_r 0 \; \forall \; x_1 \in X_1$. • (30a-b)

The passivity property (30) (Isidori, 1999; Sepulchre et al., 2012) of the reactor class (Alvarez et al., 1991): (i) is the solvability condition for the NL R stabilizing SF control problem, and (ii) delimits the attainable CL behavior with any SF control.

3.2 Steady-state (SS) uniqueness and stability

In detailed form, the CL deterministic statics (24) are written as

$$\bar{\theta}(\bar{x}_{1e} - x_1) - \delta r(x_1, x_2) = 0 \tag{31a}$$

$$\bar{\theta}(\bar{x}_{2e} - \bar{x}_2) - \eta[x_2 - \bar{x}_{2c} + k_p(x_2 - \bar{y}) + x_3] + (\delta/2) r(x_1, x_2) = 0, \;\; \bar{y} = \bar{x}_2 \tag{31b}$$

$$k_I(x_2 - \bar{y}) = 0 \tag{31c}$$

The unique-trivial solution for temperature x_2 of the integral action eq. (31c) is (32a), the passivity property (30b) ensures the unique solution (32b) for concentration x_1 of the static mass balance (31a), and the substitution of (31a) in (31b) followed by the unique solution (32c) for x_3:

$$x_2 = \bar{y} = \bar{x}_2, \quad x_1 = m(\bar{y}) \coloneqq \bar{x}_1, \quad x_3 = h(\bar{y}) = 0 \coloneqq \bar{x}_3 \tag{32a-c}$$

where

$$x_1 = m(\bar{y}) \quad \Leftrightarrow \quad \bar{\theta}(\bar{x}_{1e} - x_1) - \delta r(x_1, \bar{y}) = 0 \tag{32d}$$

$$h(\bar{y}) = [\bar{\theta}(\bar{x}_{2e} - \bar{y}) - \eta(\bar{y} - \bar{x}_{2c}) + (\delta/2) r(x_1, \bar{y})]/\eta = 0 \tag{32e}$$

In vector form, the unique SS solution (32a-c) of the CL statics (24) are written as

$$\bar{\boldsymbol{x}} = \boldsymbol{\beta}(\bar{y}), \quad \bar{\boldsymbol{x}} = (\bar{\boldsymbol{z}}^{\bar{T}}, 0)^T, \;\; \bar{y} = \boldsymbol{c}_z \bar{\boldsymbol{z}} \;\; \bar{\boldsymbol{z}} \in S_z \tag{33a-b}$$

where

$$\boldsymbol{\beta}(\bar{y}) = [m(\bar{y}), \bar{y}, h(\bar{y})]^T, \quad m\text{: (32d)}, \;\; h\text{: (32e)} \tag{33c}$$

is the single-valued setpoint-to-SS ($\bar{y}$-to-$\bar{\boldsymbol{x}}$) NL bifurcation map.

From the application of the Hurwitz stability criterion (Boyce and Di Prima, 1967), the SS $\bar{\boldsymbol{x}}$ (33) is stable if and only if the control gain meets the three inequalities

$$\boldsymbol{s}(\bar{y}, \boldsymbol{k}) >_r 0, \;\; \boldsymbol{s} = (s_1, s_2, s_3)^T, \;\; s_1, s_2, s_3\text{: (A4)} \tag{34}$$

with scalar functions s_1, s_2 and s_2 defined (in Appendix A) in terms of the three coefficients of the monic characteristic polynomial (A2) of the Jacobian matrix

$$\bar{\boldsymbol{J}} = \boldsymbol{J}(\bar{\boldsymbol{x}}), \qquad \boldsymbol{J}(\boldsymbol{x}) = [\partial_{\boldsymbol{x}} \boldsymbol{f}(\boldsymbol{x}, \bar{\boldsymbol{d}}, \boldsymbol{k})] \tag{35}$$

of the deterministic system (23) at its prescribed SS $\bar{\boldsymbol{x}}$. This result is stated next in proposition form

Proposition 2. The unique CL SS $\bar{\boldsymbol{x}}$ (33) is R stable if and only if the control gain is chosen to that

$$\boldsymbol{k} \in K_h = \{\boldsymbol{k} \in K | \boldsymbol{s}(\bar{y}, \boldsymbol{k}) >_r 0\} \supseteq K_m, \quad K\text{: (12c)}, \quad \boldsymbol{s}\text{: (34)}, \;\; K_m\text{: (22)}. \bullet \tag{36}$$

In (36), the Hurwitz gain set K_h is equal to or contained in the set K_m of R $\bar{\boldsymbol{x}}$-monostability. The latter case ($K_h \supset K_m$) occurs when $\bar{\boldsymbol{x}}$ has as basin of attraction the interior of a (possibly too small) spherical saddle limit cycle (Abraham and Shaw, 1992). This phenomenon: (i) has manifested itself in the deterministic reactor (23) with first-order kinetics and linear PI control (Giona and Paladino, 1994), and (ii) can happen in the deterministic reactor with linear P (Aris, 1965) and NL passive SF (Alvarez et al., 1991) control.

3.3 Closed-loop (CL) monostability

According to Lyapunov stability theory (Abraham and Shaw, 1992; Hubbard and West, 1995), the CL deterministic system (23) with $\boldsymbol{k} \in K_m$ (22) is R $\overline{\boldsymbol{x}}$-monostable (without limit cycling) if and only if there is a (single-well shaped) *Lyapunov function* (with minimum $\mathcal{L}^-$ at $\overline{\boldsymbol{x}}$)

$$V = \mathcal{L}(\boldsymbol{x}) > \mathcal{L}^- \; \forall \, \boldsymbol{x} \in X \backslash \overline{\boldsymbol{x}}, \quad \mathcal{L}(\overline{\boldsymbol{x}}) = \mathcal{L}^-, \quad \boldsymbol{\nabla}\mathcal{L}(\overline{\boldsymbol{x}}) = \boldsymbol{0} \tag{37a}$$

that decreases along the state motions

$$\dot{V} = [\boldsymbol{\nabla}\mathcal{L}(\boldsymbol{x}))\boldsymbol{f}(\boldsymbol{x}, \boldsymbol{k}, \boldsymbol{d}) < 0 \; \forall \, \boldsymbol{x} \in X \backslash \overline{\boldsymbol{x}}, \quad \dot{V} = 0 \; @ \; \boldsymbol{x} = \overline{\boldsymbol{x}}, \quad \boldsymbol{k} \in K_m\text{: (27)} \tag{37b}$$

with exponential ultimate (EU) motion bounding (Khalil, 2002; Sontag, 2008)

$$|\widetilde{\boldsymbol{x}}(t)| \leq a_x e^{-\lambda_x t} |\widetilde{\boldsymbol{x}}_o|^+ + b_x |\widetilde{\boldsymbol{d}}|^+ \leq |\widetilde{\boldsymbol{x}}|^+ \tag{38a}$$

where

$$\widetilde{\boldsymbol{x}} = \boldsymbol{x}(t) - \overline{\boldsymbol{x}}, \; \boldsymbol{x}(t)\text{: (25)}, \quad a_x > 0, \; b_x = (a_x/\lambda_x) l_{\boldsymbol{d}}^{\boldsymbol{f}} > 0 \tag{38b}$$

$$\lambda_x = 1/t_{\boldsymbol{x}} >_r 0, \;\; t_x\text{: (19b)}, \;\; |\widetilde{\boldsymbol{x}}|^+ = a_x |\widetilde{\boldsymbol{x}}_o|^+ + b_x |\widetilde{\boldsymbol{d}}|^+ \tag{38c}$$

$$|\boldsymbol{f}(\boldsymbol{x}, \boldsymbol{d}) - \boldsymbol{f}(\overline{\boldsymbol{x}}, \overline{\boldsymbol{d}})| \leq l_{\boldsymbol{x}}^{\boldsymbol{f}} |\boldsymbol{x} - \overline{\boldsymbol{x}}| + l_{\boldsymbol{d}}^{\boldsymbol{f}} |\widetilde{\boldsymbol{d}}| \; \forall \, \boldsymbol{x} \in X \tag{38d}$$

| | is the vector Euclidian norm, and $l_{\boldsymbol{d}}^{\boldsymbol{f}}$ is the Lipschitz constant of $\boldsymbol{f}$ with respect to $\boldsymbol{d}$.

If admissible size ($|\widetilde{\boldsymbol{x}}_o|^+$ and $|\widetilde{\boldsymbol{d}}|^+$) deviations produce amissible state size ($|\widetilde{\boldsymbol{x}}|^+$) excursions, the SS $\overline{\boldsymbol{x}}$ said to practically (P) exponentially (E) stable (La Salle and Lefschetz, 1961).

According to the preceding developments, the control gain $\boldsymbol{k} \in K_m$ should be chosen with suggestive Hurwitz criterion-based $\boldsymbol{k} \in K_h$ (36) followed by conclusive fine tuning $\boldsymbol{k} \in K_m \subseteq K_h$ (22) with numerical simulation of the CL deterministic ODE (23). In the next section, the Lyapunov characterization (37) of deterministic CL R $\overline{\boldsymbol{x}}$-monostability will become a key ingredient in the assessment of the stochastic on deterministic dynamics dependency.

4. Closed-loop PDF dynamics

In this section, the CL state PDF motion is characterized in terms of stationary R monomodality, deterministic-diffusion time scale, and MP state and its covariance evolutions.

The dynamic FP PDE (17) is written; (i) in detailed form as

$$\partial_t \pi = \partial_{x_1}\left[\tfrac{1}{2} q_1 \partial_{x_1} \pi - f_1(\boldsymbol{x}, \boldsymbol{d})\pi\right] + \partial_{x_2}\left[\tfrac{1}{2} q_2(k_p) \partial_{x_2} \pi + \tfrac{1}{2} q_c(\boldsymbol{k}) \partial_{x_3} \pi - f_2(\boldsymbol{x}, \boldsymbol{d}, k_p)\pi\right] \tag{39a}$$

$$+\partial_{x_3}\left[\tfrac{1}{2} q_3(\boldsymbol{k}) \partial_{x_3} \pi + \tfrac{1}{2} q_c(\boldsymbol{k}) \partial_{x_2} \pi - f_3(\boldsymbol{x}, k_I)\pi\right], \quad q_1, q_2, q_3, q_c\text{: (14h)}$$

$$\pi(x_1, x_2, x_3, 0) = \pi_o(x_1, x_2, x_3), \qquad \int_{x_1^-}^{x_1^+} \int_{x_2^-}^{x_2^+} \int_{x_3^-}^{x_3^+} \pi(x_1, x_2, x_3, t) dx_1 dx_2 dx_3 = 1 \tag{39b-c}$$

$$\left[\tfrac{1}{2} q_1 \partial_{x_1} \pi - f_1(\boldsymbol{x}, \boldsymbol{d})\pi\right]_{x_1^\pm} = 0, \quad \left[\tfrac{1}{2} q_2(k_p) \partial_{x_2} \pi + \tfrac{1}{2} q_c(\boldsymbol{k}) \partial_{x_3} \pi - f_2(\boldsymbol{x}, \boldsymbol{d}, k_p)\pi\right]_{x_2^\pm} = 0 \tag{39d-e}$$

$$\left[\tfrac{1}{2} q_3(\boldsymbol{k}) \partial_{x_3} \pi + \tfrac{1}{2} q_c(\boldsymbol{k}) \partial_{x_2} \pi - f_3(\boldsymbol{x}, k_I)\pi\right]_{x_3^\pm} = 0 \tag{39f}$$

and (ii) in transport-reaction form as (Alvarez et al., 2018)

$$\partial_t \pi = \tfrac{1}{2} \boldsymbol{\nabla}^T \boldsymbol{Q}(\boldsymbol{k}) \boldsymbol{\nabla} \pi - \boldsymbol{f}(\boldsymbol{x}, \boldsymbol{d}, \boldsymbol{k}) \cdot \boldsymbol{\nabla} \pi + [\boldsymbol{\nabla} \cdot \boldsymbol{f}(\boldsymbol{x}, \boldsymbol{d}, \boldsymbol{k})]\pi, \;\; \boldsymbol{x} \in \mathcal{I}_X, \;\; \boldsymbol{Q}\text{: (14h)}, \;\; \boldsymbol{f}\text{: (15c)} \tag{40a}$$

$\frac{1}{2}\boldsymbol{Q}(\boldsymbol{k})\boldsymbol{\nabla}\pi - \boldsymbol{f}(\boldsymbol{x},\boldsymbol{d},\boldsymbol{k})\pi = \boldsymbol{0}, \boldsymbol{x} \in \mathcal{B}_{\mathcal{X}}, \quad \pi(\boldsymbol{x},0) = \pi_o(\boldsymbol{x}), \quad \int_{\mathcal{X}} \pi(\boldsymbol{x},t)d\boldsymbol{x} = 1$ (40b)

From a chemical reactor engineering perspective, the CL reactor CL FP PDE (40) describes the dynamic conservation of probability over the tridimensional space $\mathcal{X}$ with impermeable bounday $\mathcal{B}_{\mathcal{X}}$, and rate of change terms [in the RHS of (40a)] due to: (i) *Fick-like linear* transport $(1/2)\boldsymbol{\nabla}^T\boldsymbol{Q}\boldsymbol{\nabla}\pi$ with *allotropic diffusion* matrix $\boldsymbol{Q}$, (ii) *convective transport* $\boldsymbol{f}\cdot\boldsymbol{\nabla}\pi$ with nonlinear space-dependent flow field $\boldsymbol{f}$, and (iii) *1st-order reaction-like probability generation* $(\boldsymbol{\nabla}\cdot\boldsymbol{f})\pi$ proportional to the probability "concentration" π and with NL dependency on the "position" $\boldsymbol{x}$. The 3-dimensional FP PDE (40) can be solved numerically with specialized methods (LeVeque, 1992) or software packages (e.g., Ansys®, Comsol Multiphysics®).

4.1 Robust stationary state PDF monomodality

Here, the correspondence between CL stochastic stationary state PDF monomodality and deterministic monostability is established by combining the characterizations of: (i) deterministic monostability with Lyapunov theory (37), and (ii) the state PDF with the fluctuation dissipation relationship (Ao, 2003; Kwon et al., 2005; Wang et al., 2006) and functional analysis tools (Markowich and Villani, 2000; Frank, 2006).

In Boltzmann-Gibbs form, the unique state PDF solution of the of the stationary FP PDE (20) is given by (Wang et al., 2006)

$\bar{\pi}(\boldsymbol{x}) = ae^{-\phi(\boldsymbol{x})}, \ \boldsymbol{x} \in \mathcal{X}, \quad \boldsymbol{\nabla}\phi(\boldsymbol{x}) = -\boldsymbol{G}^{-1}(\boldsymbol{x})\boldsymbol{f}(\boldsymbol{x},\bar{\boldsymbol{d}}), \quad \det \boldsymbol{G} \neq \boldsymbol{0}$ (41a-b)

where a is a normalization constant, and the 9-entry of the $3x3$ matrix $\boldsymbol{G}$ satisfies: (i) the fluctuation-dissipation relationship (with 9 algebraic equations)

$\boldsymbol{G}(\boldsymbol{x}) + \boldsymbol{G}^T(\boldsymbol{x}) = \boldsymbol{Q}(\boldsymbol{k})$ (41c)

and (ii) the irrotationality condition (with 3 hyperbolic linear PDEs):

$\boldsymbol{\nabla} \times [\boldsymbol{G}^{-1}(\boldsymbol{x})\boldsymbol{f}(\boldsymbol{x},\bar{\boldsymbol{d}})] = \boldsymbol{0}$ (41d)

When the stationary state PDF

$\bar{\pi}(\boldsymbol{x}) < \bar{\pi}^+ = \bar{\pi}(\bar{\boldsymbol{x}}_m) \ \forall \ \boldsymbol{x} \in \mathcal{X}\backslash\bar{\boldsymbol{x}}_m, \ \boldsymbol{\nabla}\bar{\pi}(\bar{\boldsymbol{x}}_m) = 0$

is R $\bar{\boldsymbol{x}}_m$-monomodal (with maximum $\bar{\pi}^+$ at $\bar{\boldsymbol{x}}_m$): (i) by (41), the stochastic potential

$\phi(\boldsymbol{x}) = -\ln\bar{\pi}(\boldsymbol{x})/a > \phi^- = \phi(\bar{\boldsymbol{x}}_m) \ \forall \ \boldsymbol{x} \in \mathcal{X}\backslash\bar{\boldsymbol{x}}_m, \quad \boldsymbol{\nabla}\phi(\bar{\boldsymbol{x}}_m) = \boldsymbol{0}$ (42)

is single-well shaped (with minimum ϕ^- at $\bar{\boldsymbol{x}}_m$), and (ii) the deterministic system (23) can be expressed in gradient form (Hirsch and Smale, 1974)

$\dot{\boldsymbol{x}} = -\boldsymbol{G}(\boldsymbol{x})\boldsymbol{\nabla}\phi(\boldsymbol{x}), \ \boldsymbol{x}(0) = \boldsymbol{x}_o$ (43a)

with the stochastic potential as Lyapunov function

$V = \mathcal{L}(\boldsymbol{x}) := \phi(\boldsymbol{x}), \ \phi$**:** (42) (43b)

$\dot{V} = -\boldsymbol{\nabla}^T\phi(\boldsymbol{x})[\boldsymbol{Q}(\boldsymbol{k})]\boldsymbol{\nabla}\phi(\boldsymbol{x}) \leq 0, \quad \dot{V} = 0 \Leftrightarrow \bar{\boldsymbol{x}} = \bar{\boldsymbol{x}}_m$ (43c)

According to the stochastic Boltzmann-Gibbs PDF (41) and the deterministic Lyapunov characterization (37), monostability is necessary and sufficient for monomodality. This result is stated in the next proposition.

Proposition 3. The CL stochastic stationary state PDF $\bar{\pi}(\boldsymbol{x})$ (41) is R $\bar{x}_m$-monomodal over $\mathcal{X}$ if and only if the CL deterministic system (23) is R $\bar{x}_m$-monostable over $\mathcal{X}$. •

Differently from a previous study (Alvarez et al., 2018) on the OL 2-state stochastic reactor (3) where the correspondence between state PDF monomodality and deterministic monostability was established with the analytic solution of the 2D FP PDE (10), here the same correspondence for the 3-state CL stochastic reactor (15) has been obtained (Proposition 3) with a direct method that: (i) combines stochastic fluctuation-dissipation (41) and deterministic Lyapunov stability (37), and (ii) does not require the difficult or infeasible task of analytically solving the 3D FP PDE (39).

4.2 Transient behavior

When the stationary state PDF $\bar{\pi}(\boldsymbol{x})$ is R $\overline{\boldsymbol{x}}_m$-monomodal, by the generic linearity-stability property (Risken, 1996; Gardiner, 1997) of the FP PDE (39) the state PDF motion $\pi(\boldsymbol{x}, t)$ (16) R converges to $\bar{\pi}(\boldsymbol{x})$: (i) along deterministic (t_x) and diffusion (t_d) time scales, without metastability, and (ii) with exponential ultimate (EU) bounding (Markowich and Villani, 2000; Frank, 2006)

$$|\tilde{\pi}(t)|_H \leq a_\pi e^{-\lambda_\pi t}|\tilde{\pi}_o|_H^+ + b_\pi|\widetilde{\boldsymbol{d}}|^+ \leq |\tilde{\pi}|_H^+, \qquad a_\pi, b_\pi, \lambda_\pi > 0 \tag{44a}$$

where

$$\tilde{\pi}(t) \coloneqq \pi(\boldsymbol{x}, t) - \bar{\pi}(\boldsymbol{x}), \qquad |\tilde{\pi}_o|_H^+ \leq |\tilde{\pi}_o|_H^+, \qquad |\widetilde{\boldsymbol{d}}(t)| \leq |\widetilde{\boldsymbol{d}}|^+ \tag{44b}$$

$$|\tilde{\pi}|_H^+ = a_\pi|\tilde{\pi}_o|_H^+ + b_\pi|\widetilde{\boldsymbol{d}}|^+, \quad b_\pi = (a_\pi/\lambda_\pi)l_{\boldsymbol{d}}^{\mathcal{F}}, \quad \lambda_\pi \approx 1/t_d,\ t_d \geq t_x,\ \ t_d\text{: (19b)} \tag{44c}$$

$$|\mathcal{F}(\pi, \boldsymbol{d}) - \mathcal{F}(\bar{\pi}, \overline{\boldsymbol{d}})| \leq l_\pi^{\mathcal{F}}|\boldsymbol{x} - \overline{\boldsymbol{x}}| + l_{\boldsymbol{d}}^{\mathcal{F}}|\widetilde{\boldsymbol{d}}|, \tag{44d}$$

$|\ |$ (or $|\ |_H$) is the Euclidian vector (or Hilbert function) norm, and $l_a^{\mathcal{F}}$ is the Lipschitz constant of $\mathcal{F}$ with respect to its argument a.

If admissible size ($|\tilde{\pi}_o|_H^+$ and $|\widetilde{\boldsymbol{d}}|^+$) deviations produce amissible PDE motion deviations ($\tilde{\pi}$) with admissible size ($|\tilde{\pi}|_H^+$), the nominal stationary state PDF $\bar{\pi}$ (41a) is said to be practically (P) EU stable (La Salle and Lefschetz, 1961). The employment of the R state motion convergence property in the context of a PDE reactor model can be seen in (Franco de los Reyes et al., 2020).

On the basis of (44), the mode ($\widetilde{\boldsymbol{x}}_m$) and control ($\tilde{u}_m$) deviations are EU bounded as

$$|\widetilde{\boldsymbol{x}}_m(t)| \leq l_{x_m}^{\boldsymbol{m}_x}(a_\pi e^{-\lambda_\pi t}|\tilde{\pi}_o|_H^+ + b_\pi|\widetilde{\boldsymbol{d}}|^+) \leq l_{x_m}^{\boldsymbol{m}_x}|\tilde{\pi}|_H^+ \tag{45a}$$

$$|\tilde{u}_m(t)| \leq l_{x_m}^{c_u}(a_\pi e^{-\lambda_\pi t}|\tilde{\pi}_o|_H^+ + b_\pi|\widetilde{\boldsymbol{d}}|^+) \leq l_{x_m}^{c_u}|\tilde{\pi}|_H^+ \tag{45b}$$

where

$$\widetilde{\boldsymbol{x}}_m = \boldsymbol{x}_m(t) - \overline{\boldsymbol{x}}, \ \ \boldsymbol{m}_x(\bar{\pi}) = \overline{\boldsymbol{x}}_m = \overline{\boldsymbol{x}}, \qquad |\boldsymbol{m}_x(\pi) - \boldsymbol{m}_x(\bar{\pi})| \leq l_\pi^{\boldsymbol{m}_x}|\tilde{\pi}| \tag{45c}$$

$$\tilde{u}_m = u_m(t) - \bar{u}, \ m_u(\bar{v}_m) = \bar{u}_m = \bar{u}, \ |m_u(\boldsymbol{x}_m) - m_u(\overline{\boldsymbol{x}}_m)| \leq k_{x_m}^{c_u}|\widetilde{\boldsymbol{x}}_m|, \quad k_{x_m}^{c_u} = (1 + k_p^2)^{1/2} \tag{45d}$$

The preceding functional analysis-based characterization of PDF and mode evolutions over deterministic-diffusion time biscale (t_π) is simpler and more complete than the in-probability mean-state evolution over deterministic scale employed in the stochastic NL passive stabilizing control based on the FP PDE and a HJI PDE (Krstic and Deng, 1988).

5. State and control mode evolutions

Here the state and control modes and their covariance evolutions are: (i) characterized according to the FP PDE (39), and (ii) approximated (in a practical IS convergence sense) with an ODE.

5.1 FP PDE-based mode evolution

The state PDF mode evolution $\boldsymbol{x}_m$ and its rate of change $\boldsymbol{v}_m$ are determined by the FP PDE (39) (Jazwinski, 1970) with the output map (46b):

$$\partial_t \pi = \mathcal{F}(\pi, \boldsymbol{d}), \quad \boldsymbol{\mathcal{B}}(\pi, \boldsymbol{d}) = \boldsymbol{0}, \quad \pi(0) = \pi_o(\boldsymbol{x}) \tag{46a}$$

$$\boldsymbol{x}_m = \boldsymbol{m}_x(\pi), \quad u_m = \boldsymbol{c}_u(\boldsymbol{x}_m) \tag{46b}$$

In a way that is analogous to the way in which a geometric NLSF controller is constructed (Isidori, 1999) and along FP PDE analysis ideas (Jazwinski, 1970), the time derivation of the output map $\boldsymbol{m}_x$ along the state PDF motion π yields the next proposition in terms the NL vector

$$\boldsymbol{\varrho}_\pi(\boldsymbol{x}_m, \boldsymbol{d}) = [\boldsymbol{\varrho}(\pi, \boldsymbol{d})]_{x=x_m}, \qquad \boldsymbol{\varrho}_{\bar{\pi}}(\bar{\boldsymbol{x}}_m, \bar{\boldsymbol{d}}) = \boldsymbol{0}, \qquad \bar{\boldsymbol{x}}_m = \bar{\boldsymbol{x}} \tag{47a}$$

$$|\boldsymbol{\varrho}_\pi(\pi, \boldsymbol{d})| \leq l_{\boldsymbol{x}_m}^{\boldsymbol{\varrho}_\pi} |\tilde{\boldsymbol{x}}_m| + l_{\boldsymbol{d}}^{\boldsymbol{\varrho}_\pi} |\tilde{\boldsymbol{d}}|, \qquad l_{\boldsymbol{x}_m}^{\boldsymbol{\varrho}_\pi} = l_\pi^{\boldsymbol{\varrho}} \, l_{\boldsymbol{x}_m}^{\pi} |\tilde{\boldsymbol{x}}_m|^+, \quad l_{\boldsymbol{x}_m}^{\pi} = \lambda_{\bar{H}}^{+} + k_{\boldsymbol{x}_m}^{o}, \; l_{\boldsymbol{d}}^{\boldsymbol{\varrho}_\pi} = l_\pi^{\boldsymbol{\varrho}} \, l_{\boldsymbol{d}}^{\pi} \tag{47b}$$

where

$$\boldsymbol{\varrho}(\pi, \boldsymbol{d}) = (\boldsymbol{\mathcal{H}}\pi)^{-\boldsymbol{1}}\{[\boldsymbol{\mathcal{H}}\boldsymbol{f}(\boldsymbol{x}, \boldsymbol{d})]\pi - (1/2)\boldsymbol{\mathcal{H}}(\boldsymbol{Q}\boldsymbol{\nabla}\pi)\}, \; \boldsymbol{\varrho}(\bar{\pi}, \bar{\boldsymbol{d}}) = \boldsymbol{0}, \quad \boldsymbol{\nabla}, \boldsymbol{\mathcal{H}}\text{: (18e)} \tag{47c}$$

$$|\boldsymbol{\varrho}(\pi, \boldsymbol{d})| \leq l_\pi^{\boldsymbol{\varrho}} |\tilde{\pi}|_{\bar{H}}^{+} + l_{\boldsymbol{d}}^{\boldsymbol{\varrho}} |\tilde{\boldsymbol{d}}|, \quad \boldsymbol{\varrho}(\pi, \boldsymbol{d}) = \boldsymbol{0} \text{ if } \pi \text{ is symmetric}, \quad \boldsymbol{Q}\text{: (14h)} \tag{47d}$$

$\boldsymbol{\varrho}_\pi$ vanishes at $(\bar{\boldsymbol{x}}_m, \bar{\boldsymbol{d}})$, and $\boldsymbol{\varrho}$ depends in a complex way (through up to 2nd and 3rd-order partial derivatives of the convective field $\boldsymbol{f}$ and the state PDF π, respectively) on the PDF geometry at $\boldsymbol{x}_m$.

Proposition 4 (Proof in Appendix B). The R EU convergent state (48a) and control (48b) mode evolutions satisfy the ODE-based system [driven through $\boldsymbol{\varrho}_\pi$ by driven by the state PDF π of the FP PDE (39)]

$$\dot{\boldsymbol{x}}_m = \boldsymbol{f}(\boldsymbol{x}_m, \boldsymbol{d}) + \boldsymbol{\varrho}_\pi(\boldsymbol{x}_m, \boldsymbol{d}), \; \boldsymbol{x}_m(0) = \boldsymbol{x}_{mo}; \;\; u_m = \boldsymbol{c}_u(\boldsymbol{x}_m) \tag{48a-b}$$

where

$\boldsymbol{x}_{mo} = \boldsymbol{m}_x(\pi_o)$, $\boldsymbol{f}$: (14e-f) $\boldsymbol{\varrho}_\pi$: (47c), $\boldsymbol{m}_x$: (18a), $\boldsymbol{c}_u$: (14g). •

According to (48a), the state mode rate of change $(\boldsymbol{f} + \boldsymbol{\varrho}_\pi)$ depends on the state PDF π of the FP PDE (46a), and has two components: (i) the deterministic vector field $\boldsymbol{f}$ (14) that does not depend on π, and (ii) the term $\boldsymbol{\varrho}_\pi$ that depends (47) on the geometry of π at the state mode $\boldsymbol{x}_m$. According to (48b), the control mode u_m is an output of the ODE (48) driven by π.

From the application (Gonzalez and Alvarez, 2005; Franco-de los Reyes, 2022) of Lyapunov's Converse Theorem (Vidyasagar, 1993) to (48a) the next proposition follows, with the definitions

$$l_m = \lambda_x - a_x l_{\boldsymbol{x}_m}^{\boldsymbol{\varrho}_\pi} > 0, \quad \lambda_\pi < l_m < \lambda_x, \quad \tilde{\boldsymbol{x}}_m = \boldsymbol{x}_m - \bar{\boldsymbol{x}}_m, \quad l_{\boldsymbol{x}_m}^{\boldsymbol{\varrho}_\pi}\text{: (47b)} \tag{49a}$$

$b_m = (l_{\boldsymbol{d}}^{\boldsymbol{f}} + l_{\boldsymbol{d}}^{\boldsymbol{\varrho}_\pi})/l_m, \qquad |\widetilde{\boldsymbol{x}}_m|^+ = a_x|\widetilde{\boldsymbol{x}}_{mo}|^+ + b_m|\widetilde{\boldsymbol{d}}|^+, \qquad l_{\boldsymbol{d}}^{\boldsymbol{f}}$: (38d) (49b)

where

$\boldsymbol{\varrho}_\pi = 0 \Rightarrow (l_m, b_m) = (\lambda_x, b_x), \ \ (\lambda_x, b_x)$: (38b-c) (49c)

Proposition 5 (Proof in Appendix C). The R EU convergent state (48a) and control (48b) mode evolutions are EU bounded as:

$|\widetilde{\boldsymbol{x}}_m(t)| \le a_x e^{-l_m t}|\widetilde{\boldsymbol{x}}_{mo}|^+ + b_m|\widetilde{\boldsymbol{d}}|^+ \le |\widetilde{\boldsymbol{x}}_m|^+, \qquad l_m$: (49a) (50a)

$|\tilde{u}_m(t)| \le l_{x_m}^{c_u}(a_x e^{-l_m t}|\widetilde{\boldsymbol{x}}_{mo}|^+ + b_m|\widetilde{\boldsymbol{d}}|^+) \le k_{x_m}^{c_u}|\widetilde{\boldsymbol{x}}_m|^+, \qquad k_{x_m}^{c_u}$: (45d) (50b)

where

$\widetilde{\boldsymbol{x}}_m = \boldsymbol{x}_m - \overline{\boldsymbol{x}}, \quad \tilde{u}_m = u_m - \bar{u}, \quad b_m$: (49b). (50c)

The R stability bounding of (50): (i) is less conservative than its of FP PDE-based version (44), and (ii) states that, in the limit when $\boldsymbol{\varrho}_\pi$ vanishes, the state and control modes evolve along deterministic time scale $l_m = t_x = \lambda_x$ with gain $b_m = b_x$ [(λ_x, b_x): (38b-c)].

5.2 Approximated mode and variability evolutions

Motivated by the preceding developments, let us enforce $\boldsymbol{\varrho}_\pi = 0$ in the ODE (48a) to obtain its approximation:

$\dot{\widehat{\boldsymbol{x}}}_m = \boldsymbol{f}(\widehat{\boldsymbol{x}}_m, \boldsymbol{d}), \qquad \widehat{\boldsymbol{x}}_m(0) = \widehat{\boldsymbol{x}}_{mo} \approx \boldsymbol{x}_{mo}, \ \ \boldsymbol{f}(\overline{\widehat{\boldsymbol{x}}}_m, \overline{\boldsymbol{d}}) = 0$ (51a)

with solution motions

$\widehat{\boldsymbol{x}}_m = \boldsymbol{\tau}_{\boldsymbol{x}}[t, \widehat{\boldsymbol{x}}_{mo}, \boldsymbol{d}(t)], \qquad \hat{u}_m = \boldsymbol{c}_u(\widehat{\boldsymbol{x}}_m)$ (51b)

which, by-construction (51), are EU bounded over deterministic time scale t_x as

$|\boldsymbol{e}_m(t)| \le a_x e^{-\lambda_x t}|\boldsymbol{e}_{mo}|^+ + b_x|\widetilde{\boldsymbol{d}}|^+ \le |\boldsymbol{e}_m|^+, \quad \lambda_x \approx 1/t_{\boldsymbol{x}}, \quad t_x$: (18b), $\quad b_x$: (38b) (52a)

where

$\boldsymbol{e}_m = \widehat{\boldsymbol{x}}_m(t) - \overline{\boldsymbol{x}}_m, \ \ \overline{\boldsymbol{x}}_m = \overline{\boldsymbol{x}}, \ \ |\boldsymbol{e}_m|^+ = a_x|\boldsymbol{e}_{mo}|^+ + b_x|\widetilde{\boldsymbol{d}}|^+$ (52b)

Along the notion of practical stability "when admissible disturbance size cause admissible state deviation size" (LaSalle and Lefschetz, 1961), the (R stable) mode motion $\widehat{\boldsymbol{x}}_m$(51b) is said to be ε-practically (ε-P) convergent along deterministic time scale if its relative approximation error

$e_r := \frac{||\widetilde{\boldsymbol{x}}_m|^+ - |\boldsymbol{e}_m|^+|}{|\widetilde{\boldsymbol{x}}_m|^+} \le \epsilon := 1/N, \qquad |\widetilde{\boldsymbol{x}}_m|^+$: (49b), $\quad |\boldsymbol{e}_m|^+$: (52b) (53)

is less than one in N.

This ε-P convergence property: (i) agrees with and explains the state mode evolutions over deterministic-like time scale obtained with FP PDE-based simulation in CL 1D isothermal (Baratti et al., 2018) and 2D biological (Schaum et al., 2021) reactors with proportional control.

The augmentation of (51a) with the cascaded Riccati matrix equation (54b) (Jazwinski, 1970) yields the approximated dynamics of the state ($\widehat{\boldsymbol{x}}_m$) and control ($\hat{\sigma}_u$) modes as well of their covariances ($\widehat{\boldsymbol{\Sigma}}_m$ and $\hat{\sigma}_u$):

$\dot{\widehat{\boldsymbol{x}}}_m = \boldsymbol{f}(\widehat{\boldsymbol{x}}_m, \boldsymbol{d}), \qquad \widehat{\boldsymbol{x}}_m(0) = \widehat{\boldsymbol{x}}_{mo} \approx \boldsymbol{x}_{mo}$ (54a)

$$\dot{\widehat{\boldsymbol{\Sigma}}}_m = \boldsymbol{J}(\widehat{\boldsymbol{x}}_m, \boldsymbol{d})\widehat{\boldsymbol{\Sigma}}_m + \widehat{\boldsymbol{\Sigma}}_m \boldsymbol{J}(\widehat{\boldsymbol{x}}_m, \boldsymbol{d}) + \boldsymbol{Q},\ \widehat{\boldsymbol{\Sigma}}_m(0) = \boldsymbol{\Sigma}_{mo},\ \ \boldsymbol{J}\text{: (35)} \tag{54b}$$

$$\hat{u}_m = \boldsymbol{c}_u \widehat{\boldsymbol{x}}_m, \quad \hat{\sigma}_u = \boldsymbol{v}_u(\mathrm{diag}\,\widehat{\boldsymbol{\Sigma}}_m)\,\boldsymbol{v}_u^T \tag{54c}$$

with ε-P convergent motion and output

$$(\widehat{\boldsymbol{x}}_m, \widehat{\boldsymbol{\Sigma}}_m)(t) \overset{\lambda_x}{\to} (\boldsymbol{x}_m, \boldsymbol{\Sigma}_m)(t), \quad (\hat{u}_m, \hat{\sigma}_u)(t) \overset{\lambda_x}{\to} (u_m, \sigma_u)(t), \quad \boldsymbol{x}_m, u_m, \sigma_u\text{: (18)} \tag{55}$$

and stationary regime

$$\overline{\widehat{\boldsymbol{x}}}_m = \overline{\boldsymbol{x}}_m = \overline{\boldsymbol{x}}, \quad \overline{\widehat{\boldsymbol{\Sigma}}}_m = \overline{\boldsymbol{\Sigma}}_m = \overline{\boldsymbol{\Sigma}}, \qquad \bar{\hat{\sigma}}_u = \bar{\sigma}_u \tag{56a-c}$$

$$\boldsymbol{f}(\overline{\boldsymbol{x}}_m, \overline{\boldsymbol{d}}) = \boldsymbol{0}, \quad \bar{\boldsymbol{J}}\,\overline{\boldsymbol{\Sigma}}_m + \overline{\boldsymbol{\Sigma}}_m \bar{\boldsymbol{J}}^T + \boldsymbol{Q} = \boldsymbol{0},\ \ \bar{\sigma}_u = \boldsymbol{v}_u(\mathrm{diag}\,\overline{\boldsymbol{\Sigma}}_m)\,\boldsymbol{v}_u^T, \quad \bar{\boldsymbol{J}}\text{: (35)} \tag{56d-f}$$

where $\overline{\boldsymbol{x}}$ (or $\overline{\boldsymbol{x}}_m$) is the prescribed CL deterministic SS (or state PDF mode) (32a-c) or [(43c)].

The validity of the ε-P approximation (53) will be assessed (in Section 6 on case examples) with FP PDE simulation. The analytic dependencies of the stationary state ($\overline{\boldsymbol{\Sigma}}$) and control ($\bar{\sigma}_u$) covariances on the control gains: (i) are listed in Appendix D, and (ii) will be employed in the next section to assist the gain tuning of the examples.

5.3 Interpretation of the PI control

As an important conceptual conclusion of the present study, here the industrial-type PI control for the exothermic reactor class (3) is interpreted within the FP theory-based modeling framework.

The CL stochastic dynamics of the industrial PI temperature controller (12) is an output (57c) of the CL FP PDE (57a):

$$\partial_t \pi = \mathcal{F}(\pi, \boldsymbol{d}), \ \ \boldsymbol{\mathcal{B}}(\pi, \boldsymbol{d}) = \boldsymbol{0}, \ \ \pi(0) = \pi_o(\boldsymbol{x}), \ \ v(u,t) = h[\pi(\boldsymbol{x}, t)] \tag{57a-b}$$

$$u_m = PI(y_m), \quad y_m = \boldsymbol{c}_y \boldsymbol{x}_m, \quad \boldsymbol{x}_m = \boldsymbol{m}_x(\pi) \tag{57c-e}$$

On the basis of the most probable temperature measurement y_m, the PI control (57d) applies the most probable value u_m of the control PDF $v(u,t)$. The effect of mass-heat balance, actuator, and measurement noises is accounted for by the noise covariance matrix $\boldsymbol{Q}$ (14h) of the FP PDE (57a) that generates the state (π) and control (v) PDFs.

Hitherto, the technical developments have been executed with the standard notation employed in the literature: denoting the deterministic and random variables of the ODE (23) and SDE (15) with the same symbol set $\{u, \boldsymbol{x}, y\}$. In Table 2 the deterministic (12a) and stochastic (13a) PI control variants are presented with explicitly differentiation of deterministic ($\boldsymbol{x}_d$) and random ($\boldsymbol{x}_s$) states.

Table 2. Deterministic and stochastic PI controls

	Deterministic	**Stochastic**	
PI control	$u_d = PI(y_d)$	$u_s = PI(y_s + w_y) + \xi_u$	$u_m = PI(y_m)$
	u_d, y_d: deterministic	u_s, y_s: random	u_m, y_m: PDF modes
Measurement	$y_d = \boldsymbol{c}_y \boldsymbol{x}_d$	$y_s = \boldsymbol{c}_y \boldsymbol{x}_s + w_y$	$y_m = \boldsymbol{c}_y \boldsymbol{x}_m$
Dynamics	**ODE** (23): $\dot{\boldsymbol{x}}_d = \boldsymbol{f}(\boldsymbol{x}_d, \boldsymbol{d})$	**SDE** (15): $\dot{\boldsymbol{x}}_d = \boldsymbol{f}(\boldsymbol{x}_d, \boldsymbol{d}) + \boldsymbol{w}$	**FP PDE** (39): $\boldsymbol{x}_m = \boldsymbol{m}_x(\pi)$

	$\boldsymbol{x}_d(0) = \boldsymbol{x}_{do}$	$\boldsymbol{x}_s(0) = \mathcal{R}[\pi_o(\boldsymbol{x}_s)]$	$\partial_t \pi = \mathcal{F}(\pi, \boldsymbol{d})$ $\boldsymbol{\mathcal{B}}(\pi, \boldsymbol{d}) = \boldsymbol{0}$ $\pi(\boldsymbol{x}, 0) = \pi_o(\boldsymbol{x})$
State	$\boldsymbol{x}_d$: deterministic	$\boldsymbol{x}_s$: random	π: PDF

6. Illustration with indicative examples

Here, the main theoretical developments and findings of Sections 3 to 5 are illustrated with analytic formula application and finite volume method-based (Balzano et al., 2010) CL 3-state FP PDE (39) numerical simulation.

On the basis of a previous study (Alvarez et al., 2018), the OL 2-state stochastic reactor class (3) was set with: (i) reaction rate with first-order kinetics and Arrhenius temperature dependency, i.e.,

$$r(x_1, x_2) = x_1 e^{\varepsilon_a (1 - 1/x_2)}, \quad \varepsilon_a = E_a/(R_g T_r) = 25, \quad \bar{x}_{1e} = \bar{x}_{2e} = \bar{x}_{2c} = 1 \tag{58a-c}$$

and (ii) realistic background and instrument measurement noise standard deviations

$$s_1 := \sqrt{q_1} = 1.14 \cdot 10^{-2}, \; s_2 := \sqrt{q_2} = 6.32 \cdot 10^{-3}, \; s_u := \sqrt{q_u} = 0, \; s_y := \sqrt{q_y} = 2 \cdot 10^{-4} \tag{59a-d}$$

that determine the CL noise covariance 3x3 matrix $\boldsymbol{Q}(\boldsymbol{k})$ (14h).

Figure 1 shows that, over its Damköhler-Stanton (δ-η) parameter space, the OL 2-state stochastic reactor (8) has regions of monomodal, bimodal and vulcanoid stationary 2-state PDF $\bar{\varsigma}(\boldsymbol{z})$ (11a) (Alvarez et al., 2018): (i) underlain by deterministic monostability, bistability, and limit cycling, respectively, and (ii) delimited by deterministic saddle-node (S) (dashed line) and Hopf (H) (continuous line) bifurcation curves.

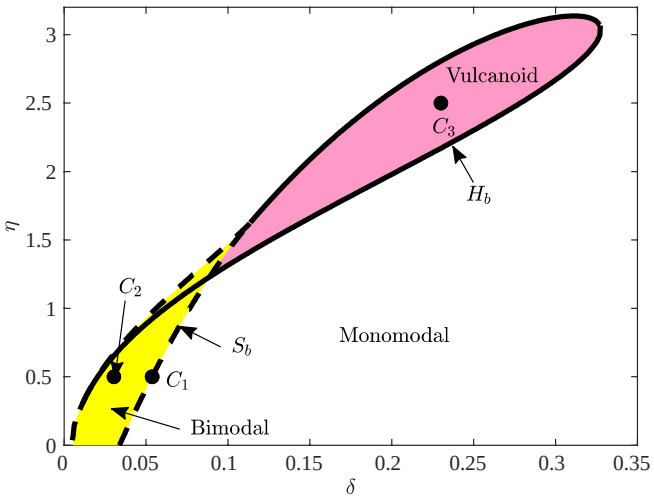

Figure 1. Stationary state PDF [$\bar{\varsigma}(\boldsymbol{z})$ (11a)] behavior regions of the reactor class (3), in the Damköhler-Stanton parameter space delimited by deterministic saddle-node (S_b) (- - - -) and Hopf (H_b) (——) bifurcation: (i) monomodal (white), (ii) bimodal (yellow), and (iii) vulcanoid (pink). Indicative examples (Table 3) (•): (i) C_1 (fragile bimodality), (ii) C_2 (robust bimodality), and (iii) C_3 (robust vulcanoid).

Table 3. OL 2-state and CL 3-state stationary PDF characteristics of the case examples.

		Stationary state PDF			
Case		**Open-loop**			**Closed-loop**
	δ: **Damköhler** η: **Stanton**		**Extremum set**: $\mathcal{E}_o$ **Setpoint:** $\bar{y} = \boldsymbol{c}_z \bar{\boldsymbol{z}}_m^-$	**Target Extremum**	**Robust monomodal state PDF**
C_1	$\delta = 0.0537$ $\eta = 0.5$	**Bimodal** Fragile Alo-probable	$\mathcal{E}_o = \{\bar{\boldsymbol{z}}_m^-, \bar{\boldsymbol{z}}_s, \bar{\boldsymbol{z}}_m^+\}$ $\bar{\boldsymbol{z}}_m^-, \bar{\boldsymbol{z}}_m^+$: Highly probable modes $\bar{y} = 1.05235$ (of $\bar{\boldsymbol{z}}_m$)	$\bar{\boldsymbol{z}}_m^-$: Least probable mode	$\mathcal{E} = \bar{\boldsymbol{x}}_m$ $\bar{\boldsymbol{x}}_m = \begin{bmatrix} \bar{\boldsymbol{z}}_m \\ 0 \end{bmatrix}$ $\bar{y} = \boldsymbol{c}_x \bar{\boldsymbol{x}}_m$
C_2	$\delta = 0.030903$ $\eta = 0.5$	**Bimodal** Robust Equi-probable	$\mathcal{E}_o = \{\bar{\boldsymbol{z}}_m^-, \bar{\boldsymbol{z}}_s, \bar{\boldsymbol{z}}_m^+\}$ $\bar{\boldsymbol{z}}_m^-, \bar{\boldsymbol{z}}_m^+$: Highly probable modes $\bar{y} = 1.15227$ (of $\bar{\boldsymbol{z}}_s$)	$\bar{\boldsymbol{z}}_s$: Almost null probable saddle	
C_3	$\delta = 0.23$ $\eta = 2.5$	**Vulcanoid** Robust	$\mathcal{E}_o = \{\bar{\boldsymbol{z}}_m, \boldsymbol{l}\}$ $\boldsymbol{l}$: Highly probable rim $\bar{y} = 1.09627$ (of $\bar{\boldsymbol{z}}_m$)	$\bar{\boldsymbol{z}}_m$: Almost null probable bottom	

The tree indicative case examples listed in Table 3 (dots in Figure 1) with complex (non-monomodal) OL PDFs and possibility of metastability (in cases C_1 and C_2) were chosen [geometric and denomination details can be seen in (Alvarez et al., 2018)].

- Case C_1 with OL fragile aloprobable bimodality (underlain by deterministic aloattractive bistability), and the least probable mode as target CL extremum.
- Case C_2 with OL robustly equiprobable bimodality (underlain by deterministic equiattractive bistability), and the almost null probable saddle as target CL extremum.
- Case C_3 with OL robust vulcanoid (underlain by a deterministic limit cycle), and the almost null probable bottom minimum as target CL extremum.

In the three cases, CL state PDF dynamics must be attained, with: (i) robustly monomodal stationary 3-state PDF $\bar{\pi}(\boldsymbol{x})$ with prescribed mode $\bar{\boldsymbol{x}}_m = \bar{\boldsymbol{x}}$ (43c) determined by the OL 2-state extremum $\bar{\boldsymbol{z}}$ (4b), (ii) preclusion of metastability (19b), and (iii) an adequate compromise between state mode and variability regulation speed, robustness with respect to deterministic and stochastic disturbances, and control mode-variability effort.

The dependency of the stationary concentration ($\bar{s}_1$), temperature ($\bar{s}_2$), integral action ($\bar{s}_3$) state and control ($\bar{s}_u$) standard deviations (STDs)

$$(\bar{s}_1, \bar{s}_2, \bar{s}_3, \bar{s}_u)(\boldsymbol{k}) = \left(\sqrt{\bar{\sigma}_{11}}, \sqrt{\bar{\sigma}_{22}}, \sqrt{\bar{\sigma}_{33}}, \sqrt{\bar{\sigma}_u}\right)(\boldsymbol{k}) \tag{60}$$

on PI gain vector $\boldsymbol{k}$ (12a) is given by the analytical solution (D3 in Appendix D) of the stationary Riccati equation (56e).

For application-oriented insight purpose, the proportional gain-reset time parametrization

$$\boldsymbol{\kappa} = (k_p, \tau_I)^T \in \mathcal{K}_h \subseteq \mathcal{K}_m \subset \mathcal{K}, \quad \tau_I = k_p/k_I \text{: (12c)} \tag{61a}$$

of the proportional-integral gain vector $\boldsymbol{k}$ (12) will be employed, where

$$\mathcal{K}_h = \boldsymbol{f}_{\boldsymbol{\kappa}}(K_h), \quad \boldsymbol{\kappa} = (k_p, k_p/k_I)^T \coloneqq \boldsymbol{f}_{\boldsymbol{\kappa}}(\boldsymbol{k}), \quad K\text{: (12c)},\ K_h\text{: (36)},\ K_m\text{: (22)} \tag{61b}$$

For comparative visualization purposes, the graphical displays will be done for: (i) the single-state marginal concentration, temperature, integral action, and control (18f-g) PDFs of the CL $\boldsymbol{\kappa}$-dependent 3-state PDF (39), and (ii) the concentration-temperature marginal PDF

$$\bar{\varsigma}_c(\boldsymbol{z}) \coloneqq \int_{x_3^-}^{x_3^+} \bar{\pi}(\boldsymbol{x}) dx_3, \quad \bar{\pi}\text{: (41)}, \quad \bar{\varsigma}(\boldsymbol{z})\text{: (11a)}, \quad x_3^- = -0.2, \quad x_3^+ = 0.2 \tag{62}$$

and the OL 2-state PDF (11a).

Case C_1 will examined in detail, including: (i) stationary state PDF shape, stationary state and control PDF standard deviations (STDs) dependency on gain as well as mode and its covariance evolution, and dependency of the PDF evolution on gain. Due to space limitation, for Cases C_2 and C_3 only the stationary PDF shape and the dependency of the state and control STDs on gain will be presented.

6.1 Case C_1 (OL fragile bimodal PDF)

In Case C_1 (Figure 1, Table 3): (i) the OL 2-state PDF is fragilely aloprobable bimodal with least probable mode $\bar{\boldsymbol{z}}_m^-$ as target extremum, and (ii) the controller must attain robust 3-state CL monomodality with most probable stationary state $\bar{\boldsymbol{x}}_m$ at the extremum $\boldsymbol{x}_m^-$ associated with $\bar{\boldsymbol{z}}_m^-$.

6.1.1 Gain selection

In Figure 2 are presented the analytic dependencies on the gain $\boldsymbol{\kappa} \in \mathcal{K}_h$ (61) (green subset of the bottom gain plane $\mathcal{K}$), where the necessary Hurwitz conditions (36) are met, of the concentration ($\bar{s}_1$), temperature ($\bar{s}_2$), and control ($\bar{s}_u$) standard deviations (60) of the stationary CL covariance matrix $\bar{\Sigma}$ (56b), for three measurement noise STDs s_y: (i) $= 0$ (left column), (ii) $= 2.00 \cdot 10^{-4}$ (59d) (center column, nominal value), and (iii) $= 6.32 \cdot 10^{-4}$ (right column).

According to Figure 2, for fixed integral reset time τ_I, with the increase of the proportional gain k_P: (i) the concentration standard deviation $\bar{s}_1$ (first row) decreases, reaching an asymptotic value determined by the background concentration [s_1 (59a)] and temperature measurement [(s_y) (59d)] noise STDs, (ii) the temperature standard deviation $\bar{s}_2$ (2nd row) initially decreases, reaches a minimum value, and then increases, (iii) and the control STD $\bar{s}_u$ (3rd row) grows with the gain. The increase of the temperature measurement STD s_y makes more rapid and pronounced the changes. These FP theory-based results, agree with and explain: (i) common knowledge in industrial control practice (Samad, 2017), (ii) the results obtained before with MC simulation (Ratto, 1998; Ratto and Paladino, 2000).

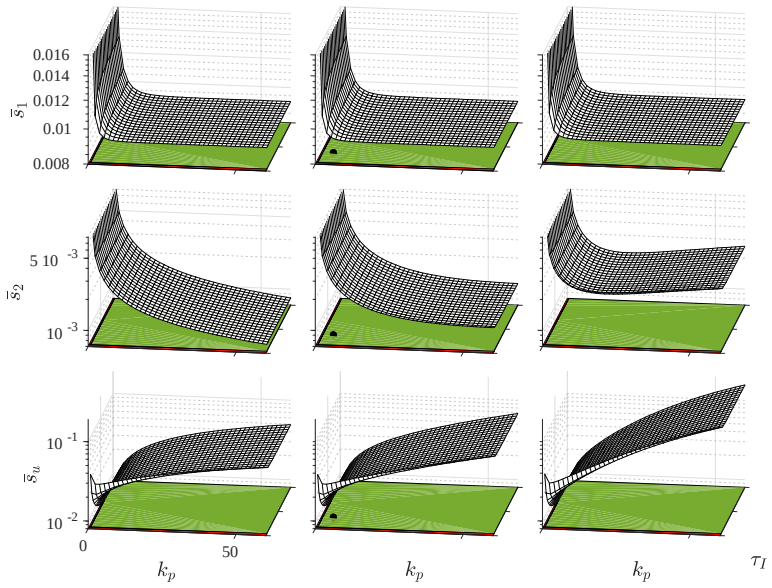

Figure 2. Dependency of the stationary concentration ($\bar{s}_1$) and temperature ($\bar{s}_2$) states as well as control ($\bar{s}_3$) PDF standard deviations on the control gain pair $\boldsymbol{\kappa} \in \mathcal{K}$ (61) for Case C_1 (Table 3) with noise STDs (59a-c). • (in bottom plane): tight control gain $\boldsymbol{\kappa}_1^t \in \mathcal{K}_h$ (63a).

Tight ($\boldsymbol{\kappa}_1^t$) and loose ($\boldsymbol{\kappa}_1^l$) gain pairs were considered

$$\boldsymbol{\kappa}_1^t = (4{,}1)^T \in \mathcal{K}_h, \quad \boldsymbol{\kappa}_1^l = (1{,}1)^T \in \mathcal{K}_h, \quad \mathcal{K}_h \subseteq \mathcal{K}_m\text{: (61)} \tag{63a-b}$$

with: (i) $\boldsymbol{\kappa}_1^t$ chosen to get an adequate compromise between regulation speed, state and control effort variances (see bottom plane of Figure 2, central column), and (ii) $\boldsymbol{\kappa}_2$ (with proportional gain four times slower, closer to the bifurcation boundary of the gain $\mathcal{K}_h$) chosen for comparison and analysis. The gain $\boldsymbol{\kappa}_1^t$ (or $\boldsymbol{\kappa}_1^l$) is away from (or close to) the boundary $\boldsymbol{s}(\bar{y}, \boldsymbol{\kappa}_i) = 0$ (34) of the Hurwitz gain set $\mathcal{K}_h$ (61b) where mono-bimodal (Figure 1) CL extremum bifurcation occurs by control gain change.

6.1.2 OL and CL stationary state PDFs

With the tight gain $\boldsymbol{\kappa}_1^t$ (63a) and noise values (59), the OL (fragilely bimodal) stationary PDF (top panel) becomes the CL (robustly monomodal) concentration and temperature marginal PDF (bottom panel) $\bar{\varsigma}_c(\boldsymbol{z})$ (62) reported in Figure 3, showing that, in agreement with the theoretical results (of Sections 3 to 5): in the open (top panel)-to-closed (bottom panel) loop passage, the least probable and nonunique 2-state OL mode $\bar{\boldsymbol{z}}_m$ becomes the unique CL mode $\bar{\boldsymbol{x}}_m$ of the monomodal almost Gaussian stationary 3-state PDF. As expected, the loose gain $\boldsymbol{\kappa}_1^l$ (63b) (with PDFs not shown for lack of space) yields larger state variance and skewness than the nominal gain $\boldsymbol{\kappa}_1^t$ (63a).

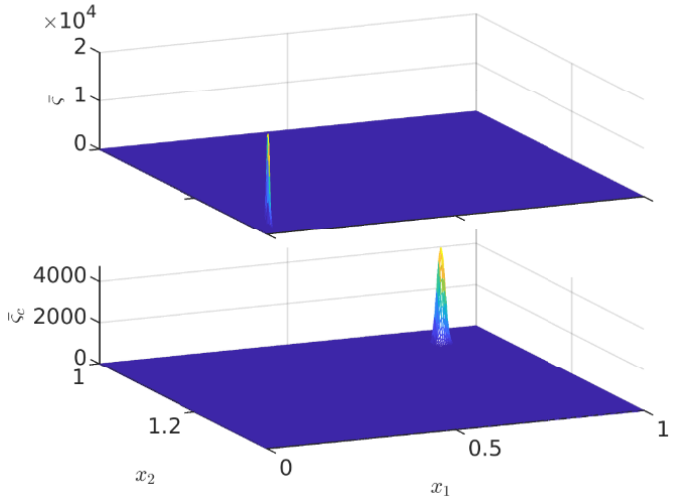

Figure 3. Stationary concentration-temperature state PDFs for Case C_1 (Table 3) with tight control gain $\boldsymbol{\kappa}_1^t$ (63a): (i) OL $\bar{\varsigma}(\boldsymbol{z})$ (11a) (top panel), and (ii) CL marginal $\bar{\varsigma}_c(\boldsymbol{z})$ (62) (bottom panel) of $\bar{\pi}(\boldsymbol{x})$ (41).

6.1.3 CL PDF transient behavior

To assess the CL state PDF (39) transients with tight [$\boldsymbol{\kappa}_1^t$ (63a)] and loose [$\boldsymbol{\kappa}_1^l$ (63b)] control gain pairs: (i) the FP PDE (39) and vector-Riccati ODE (54) systems were set with a +2% deterministic feed temperature disturbance

$$\boldsymbol{d} = (\bar{\theta}, \bar{x}_{1e}, \bar{x}_{2e} + 0.02)^T \tag{64a}$$

(ii) the FP PDE (39) was set with initial Gaussian PDF π_g whose mode $\boldsymbol{x}_{mo}$ is the target one $\overline{\boldsymbol{x}}_m$ (associated to the least probable mode $\overline{\boldsymbol{z}}_m^-$ of the OL bimodal distribution $\bar{\varsigma}(\boldsymbol{z})$ in Table 3)

$$\pi_o = \pi_g(\boldsymbol{x}), \quad \boldsymbol{m}_x(\pi_o) = \overline{\boldsymbol{x}}_m = \overline{\boldsymbol{x}}, \quad x_{3o} = 0 \tag{64b}$$

and numerically integrated with finite-volume method, and (ii) the vector-Riccati ODE (54) was set with initial zero integral action state and exact initial PDF mode and covariance

$$\hat{\boldsymbol{x}}_{mo} = \overline{\boldsymbol{x}}_m, \quad \hat{\boldsymbol{\Sigma}}_{mo} = \boldsymbol{\Sigma}_{mo}, \quad \hat{x}_{3o} = 0 \tag{64c}$$

and numerically integrated with 4th-order Runge-Kutta method.

The corresponding CL marginal PDFs evolutions (18g) are presented in Figure 4, showing that: (i) with the tight gain $\boldsymbol{\kappa}_1^t$ (63a) (left column), the 3-state CL PDF remains monomodal along the entire transient, and (ii) with the loose gain $\boldsymbol{\kappa}_1^l$ (63b) (right column), the PDF becomes bimodal at $t \approx 5$, remains bimodal up to time ≈7, and becomes monomodal thereafter. As expected, in both cases the final state PDF is monomodal. The transient monomodal (or bimodal) behavior manifests the awayness from (or closeness to) of the gain $\boldsymbol{\kappa}_1^t$ (or $\boldsymbol{\kappa}_1^l$) to the boundary $\boldsymbol{s}(\bar{y}, \boldsymbol{\kappa}_i) = 0$ (32) of the Hurwitz gain set $\mathcal{K}_h$ (63b) (where mono-bimodal CL PDF extremum bifurcation occurs, see Figure 1). The numerical FP PDE-based PDF modeling functions well in close to and away from deterministic bifurcation condition.

From a FP theory modeling perspective (Risken, 1996; Gardiner, 1997), the breakdown of the MC method in close to deterministic bifurcation condition reported in previous OL (Pell and Aris, 1969) and CL (Ratto, 1998) exothermic chemical reactor studies is explained as follows (Alvarez et al., 2018): the PDF characteristics of the infinite-dimensional FP PDE (39) cannot be -in general- captured by the finite-dimensional ODE (15) forced by a sequence of random steps (that approximate the noise $\boldsymbol{w}$).

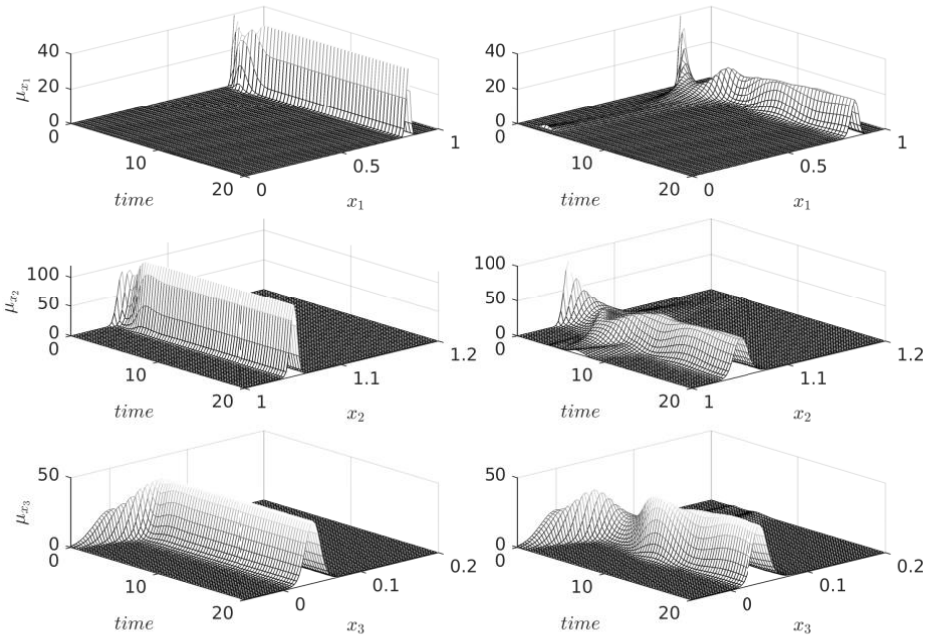

Figure 4: CL concentration (μ_{x_1}), temperature (μ_{x_2}) and integral action (μ_{x_3}) state marginal PDF evolutions (18g) of Case C_1 (Table 3) with: (i) tight gain $\boldsymbol{\kappa}_1^t \in \mathcal{K}_h$ (63a) (left column), and (ii) tight gain $\boldsymbol{\kappa}_1^l \in \mathcal{K}_h$ (63b) (right column).

6.1.4 Mode and variance evolutions

In Figure 5 are presented the actual PDE-based (46) and approximated ODE-based (54) mode transients $\boldsymbol{x}_m$ and $\widehat{\boldsymbol{x}}_m$, respectively, with tight [$\boldsymbol{\kappa}_1^t$ (63a)] and loose [$\boldsymbol{\kappa}_1^l$ (63b)] control gain pairs and input-initial condition (64), showing that: (i) with $\boldsymbol{\kappa}_1^t$, $\boldsymbol{x}_m$ (left column) evolves over almost deterministic time scale $t_x \approx 5$, and $\widehat{\boldsymbol{x}}_m$ (left column) ε-P converges (53) (with imperceptible to the eye error) to $\boldsymbol{x}_m$, and (ii) with $\boldsymbol{\kappa}_1^l$, $\boldsymbol{x}_m$ (right column) evolves over deterministic-diffusion time biscale $t_\pi \approx 25$, and $\widehat{\boldsymbol{x}}_m$ (right column) ε-P converges (53) (with admissible transient error) or not (if the error size is inadmissible) to $\boldsymbol{x}_m$, depending on the specific reactor and operation condition in actual variables and dimensions and associate model parameter uncertainties. In agreement with Proposition 5, in both gain cases, the approximated versus actual asymptotic mode error is zero.

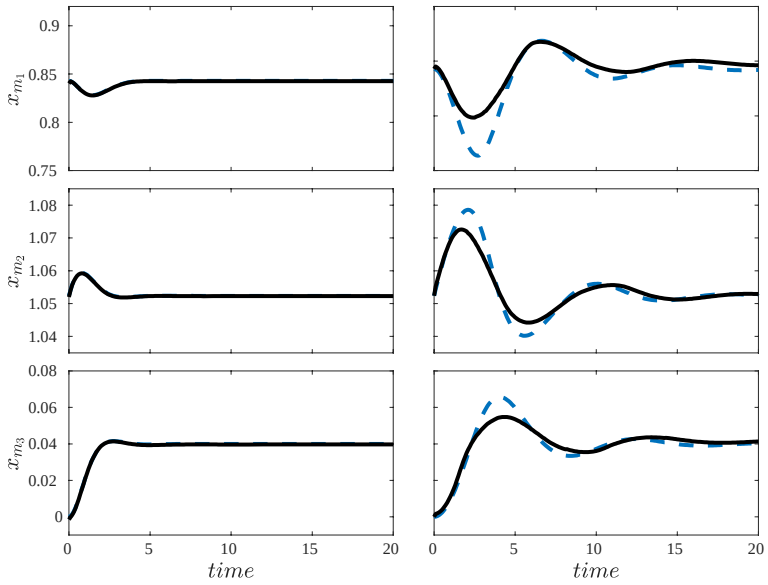

Figure 5: Actual FP PDE (46) (black line) and approximated ODE (54a)-based (blue dashed line) CL concentration, temperature, and integral action state mode evolutions for Case C_1 (Table 3) with: (i) tight gain $\boldsymbol{\kappa}_1^t \in \mathcal{K}_h$ (63a) (left panel), and (ii) loose gain $\boldsymbol{\kappa}_1^l \in \mathcal{K}_h$ (63b) (right panel).

In Figure 6 are presented the actual FP PDE-based (39) (right panel) and approximated Riccati ODE-based (54a-b) (left panel) state [μ_{x_i} (18g)] and control [ν (18f)] marginal PDFs evolutions in contour form (yellow/purple curve: most/least probable value) for the tight gain case $\boldsymbol{\kappa}_1^t$, showing (in agreement with results of Subsection 5.2 and of Figure 5) that: (i) the actual marginal state (μ_{x_i}) and control (ν) PDFs evolve over almost deterministic time scale $t_x \approx 5$, and the approximated ones $\hat{\mu}_{x_i}$ and $\hat{\nu}$ (bottom panels) ε-P converge (53) (with imperceptible to the eye error) to μ_{x_i} and ν. The agreement between Riccati-based (left panel) and numerical solution of the FP PDE (right panel) marginals is rather good at any time since the enhanced-by-feedback CL diffusion characteristic time scale is comparable to the deterministic one. This verifies the methodological proposal (Subsection 5.2) of selecting the control gain with a two-step procedure: gross tuning with the Hurwitz criterion [(36) and (61)] in the light of stationary state and control covariances (60) followed by fine tuning with stationary and transient FP PDE simulation.

The preceding results and discussion confirm and illustrate the theoretical development presented in Sections 4-5. In particular, the validity of the ε-P convergence theoretical possibility (53) for the mode transient has been validated with FP PDE simulation.

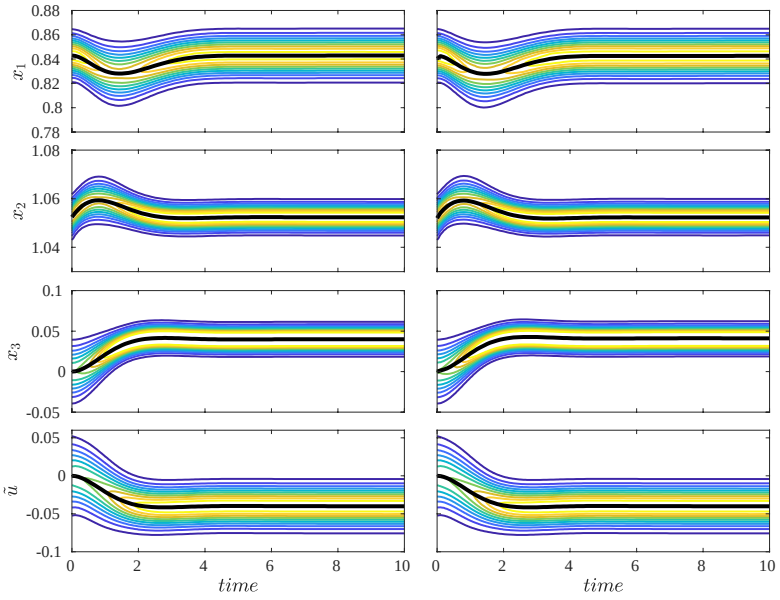

Figure 6. CL concentration (μ_{x_1}), temperature (μ_{x_2}), integral action (μ_{x_3}) and control (ν) state marginal PDF evolutions (18f-g) in contour form (black: mode, yellow/blue: most/least probable) for Case C_1 (Table 3) with tight control gain $\boldsymbol{\kappa}_1^t \in \mathcal{K}_h$ (63a), on the basis of the numerical solutions of: (ii) the Riccati ODE (54) (left panel), and (ii) the FP PDE (39) (right panel).

6.2 Case C_2 (OL robust bimodal PDF)

In case C_2 (Figure 1, Table 3): (i) the OL 2-state state PDF is robustly equiprobable bimodal, and (ii) the controller must attain R 3-state CL monomodality with most probable state at the almost null probable OL saddle.

In Figure 7, the analytic dependency on the gain $\boldsymbol{\kappa} \in \mathcal{K}_h$ (61) (green subset of the bottom gain plane $\mathcal{K}$) of the stationary concentration and temperature state as well as control STDs on gains for background noise intensity (60) are presented. The concentration STD (top panel) decreases with the proportional gain, reaching an asymptotic value determined by the background noise and temperature measurement noise STDs. The temperature STD (central panel) initially decreases with proportional, reaches a minimum, and grows thereafter. The control STD stand (bottom panel) initially decreases with proportional gain, reaches a minimum, and grow thereafter. As expected, the decrease of rest time (increase of integral gain) increases noise-to-control STD propagation.

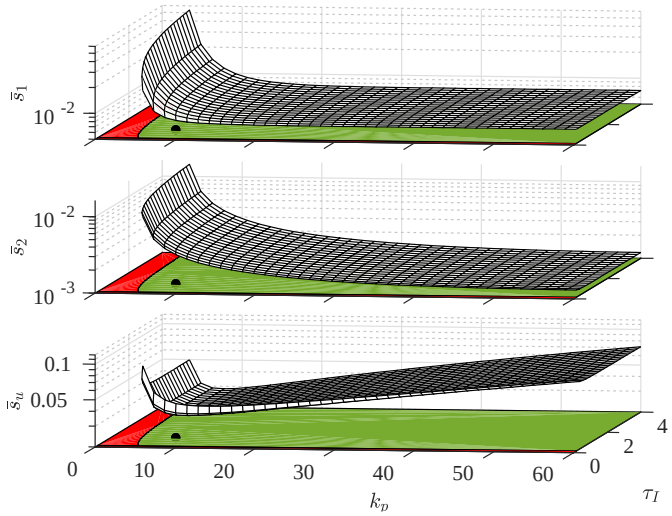

Figure 7. Dependency of the CL stationary concentration ($\bar{s}_1$) and temperature ($\bar{s}_2$) states as well as control ($\bar{s}_3$) PDF STDs on the control gain pair $\boldsymbol{\kappa} \in \mathcal{K}_h$ (61) for Case C_2 (Table 3) with noise STDs (60). • (in bottom plane $\mathcal{K}$): control gain $\boldsymbol{\kappa}_2 \in \mathcal{K}_h$ (65).

On the basis of the analytic (Appendix D) state and control standard deviation dependencies on the gain pair $\boldsymbol{\kappa}$ plotted in Figure 7 plus FP PDE simulation-based tuning, the control gain pair (dot in the bottom plane of Figure 7)

$$\boldsymbol{\kappa}_2 = (k_p, \tau_I)^T = (8, 1)^T \in \mathcal{K}_h \tag{65}$$

was chosen to get an adequate compromise between regulation speed, state and control effort modes and variances.

The resulting CL robust concentration-temperature marginal PDF $\bar{\varsigma}_c$ (62) is plotted in Figure 8 (bottom panel). In the open-to-closed loop passage the PDF saddle (associated to the unstable deterministic steady state) becomes the most probable state of a monomodal state PDF, in agreement with Proposition 3.

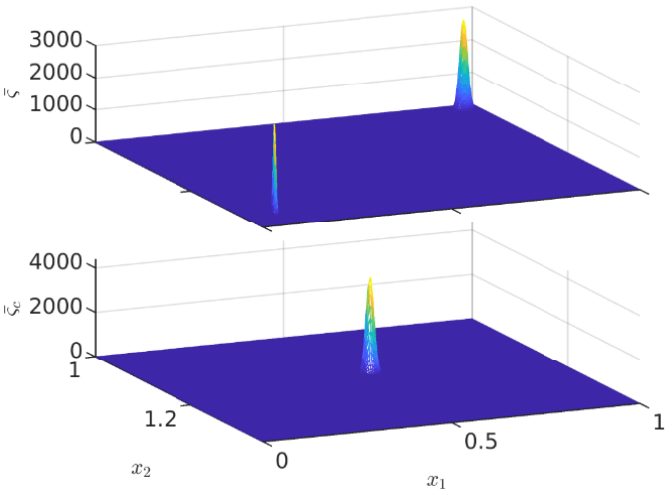

Figure 8. Stationary concentration-temperature state PDFs for Case C_2 (Table 3) with control gain $\boldsymbol{\kappa}_2 \in \mathcal{K}_h$ (65): (i) OL $\bar{\varsigma}(\boldsymbol{z})$ (11a) (top panel), and (ii) CL marginal $\bar{\varsigma}_c(\boldsymbol{z})$ (62) (bottom panel) of $\bar{\pi}(\boldsymbol{x})$ (41).

6.3 Case C_3 (OL robust vulcanoid PDF)

In case C_3 (Figure 1, Table 3): (i) the OL 2-state state PDF has vulcanoid shape, and (ii) the controller must attain R 3-state CL monomodality with most probable state at the almost null probable OL volcano bottom.

In Figure 9, the analytic dependencies on the gain $\boldsymbol{\kappa} \in \mathcal{K}_h$ (61) (green subset of the bottom gain plane $\mathcal{K}$) of the stationary concentration and temperature state as well as control STDs on control gain are plotted for the noise STDs (60). The STD on gain dependency is similar to the one (Figure 2) of Case C_1, with an important difference: the temperature STD exhibits a more pronounced minimum (at gain $k_p \approx 12$). This reflects the fact that the temperature set point of the PI control is associated with: (i) the absolute minimum (bottom point) of the OL vulcanoid PDF, and (ii) the unstable focus of the deterministic limit cycle.

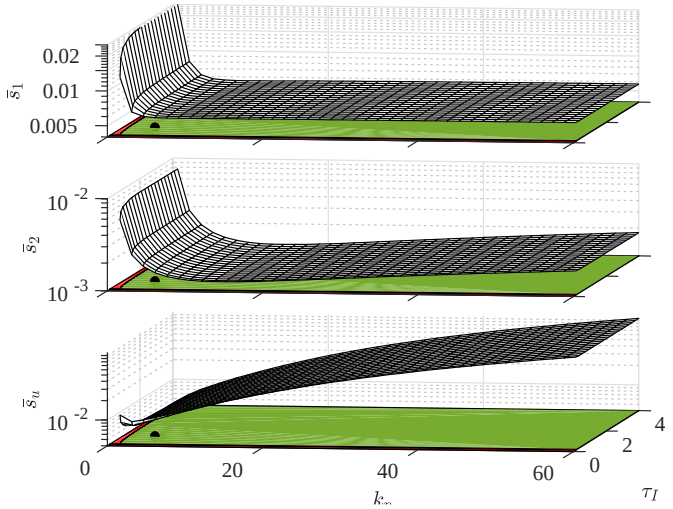

Figure 9. Dependency of the CL stationary concentration ($\bar{s}_1$) and temperature ($\bar{s}_2$) states as well as control ($\bar{s}_3$) PDF STDs on the control gain pair $\boldsymbol{\kappa} \in \mathcal{K}_h$ (61) for Case C_3 (Table 3) with noise STDs (60). • (in bottom plane $\mathcal{K}$): control gain $\boldsymbol{\kappa_3} \in \mathcal{K}_h$ (66).

On the basis of the analytic (Appendix D) state and control standard deviation dependencies on the gain pair $\boldsymbol{\kappa}$ plotted in Figure 9 followed by some FP PDE simulation-based tuning, the control gain pair (dot in the bottom plane of Figure 9)

$$\boldsymbol{\kappa}_3 = (k_p, \tau_I)^T = (4, 1)^T \in \mathcal{K}_h \tag{66}$$

was chosen to attain an adequate compromise between regulation speed, state and control effort variances.

The resulting CL stationary concentration-temperature marginal PDF $\bar{\varsigma}_c$ (62) is presented in Figure 10 (bottom panel), confirming again that -in agreement with theoretical results- in the open-to-closed loop passage the almost improbable vulcanoid PDF bottom tip (associated with the center of a deterministic OL LC) becomes the most probable state of a monomodal state PDF.

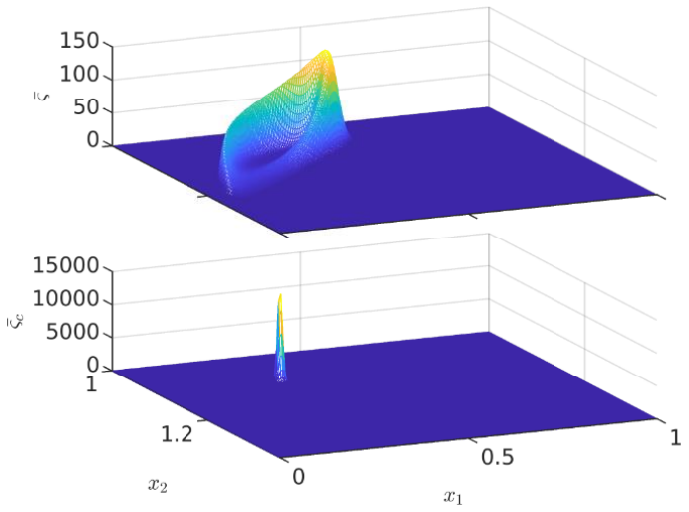

Figure 10. Stationary concentration-temperature state PDFs for Case C_3 (Table 3) with control gain $\boldsymbol{\kappa}_3$ (66): (i) OL $\bar{\varsigma}(\boldsymbol{z})$ (11a) (top panel), and (ii) CL marginal $\bar{\varsigma}_c(\boldsymbol{z})$ (62) (bottom panel) of $\bar{\pi}(\boldsymbol{x})$ (41).

7. Conclusions

The longstanding problem (Ratto, 1998; Ratto and Paladino, 2000) of assessing the CL stochastic dynamics of a class (15) of 2-state NL exothermic continuous reactors with PI temperature control has been formally resolved with Fokker Planck (FP) PDE theory. The dependency of the stochastic on deterministic dynamics was established, including the geometric correspondence between stationary state PDF and deterministic global monostability. This dependency is important to exploit the accumulated knowledge and insight on deterministic reactor NL dynamics in the stochastic dynamics assessment and PI control tuning tasks. Along pioneering studies with local FP and MC method (Ratto, 1998; Ratto and Paladino, 2000) and current industrial trends (Samad, 2017; Maxim et al., 2019), a further step towards the development of a FP theory-based joint PI-SP control design methodology for industrial reactors with complex OL PDF dynamics has been taken.

It was established that: (i) stochastic R PDF monomodalization requires deterministic passivity and the fulfillment of a control gain condition, (ii) the state PDF transient evolves along deterministic and probability diffusion time scales, with preclusion of long-term metastability, (iii) with an adequate gain choice, the most probable (MP) state and control and their variabilities evolve along almost deterministic time scale, and (iv) the industrial PI control regulates the reactor MP state by adjusting the MP control on the basis of the MP temperature measurement. The interplay between gain choice, state PDF regulation capability, and control effort was identified. An application-oriented efficient two-step gain tuning scheme was proposed: analytic formulae-based gross tuning followed by FP PDE simulation-based fine tuning.

The proposed methodology was illustrated with three indicative examples with complex OL bimodal and vulcanoid state PDFs. With FP PDE numerical simulation it was corroborated that: (i)

CL R monomodality is attained in the three cases, and (ii) the proposed methodology functions well in away from and close to deterministic bifurcation, while the MC method of previous OL (Pell and Aris, 1969) and CL (Ratto, 1998) reactor studies breaks down in close to deterministic bifurcation.

The present study is a point of departure to address in the future: (i) the optimization-based systematization of PI control gain tuning in the light of SP control, (ii) the compensation of PDF extremum shifting due to multiplicative noise (Krstic and Deng, 1988; Baratti et al., 2018), (iii) the development of the observer-based MP state control variant of the stochastic passive NL mean SF control (Krstic and Deng, 1988; Lu et al., 2022), (iv) the supplementation of the proposed PI control-based MP state regulation scheme with a noninterfering MP state estimator for setpoint adjustment in a supervisory layer (McAvoy, 2002; Maxim et al., 2019), and (v) the deterministic-to-stochastic extension of the saturated PI control with anti-windup protector (Alvarez et al., 1991; Schaum et al., 2012; Franco-de los Reyes, 2022).

References

Abraham, J.R.H., and Shaw, C.D., 1992. Dynamics: the geometry of behavior, Addison Wesley, New York.

Alvarez, J., Alvarez, J., Suarez, R., 1991. Nonlinear bounded control for a class of continuous agitated tank reactors, *Chem. Eng. Sci.* 46(12), 3235-3249. https://doi.org/10.1002/acs.717.

Alvarez, J., Baratti, R., Tronci, S., Grosso, M., Schaum, A., 2018. Global-nonlinear stochastic dynamics of a class of two-state two-parameter non-isothermal continuous stirred tank reactors. *J. of Proc. Contr*. 72, 1-16. https://doi.org/10.1016/j.jprocont.2018.07.012.

Annunziato, M., Borzì, A., Nobile, F., Tempone, R., 2014. On the Connection between the Hamilton-Jacobi-Bellman and the Fokker-Planck Control Frameworks. *Appl. Math*. 5, 2476-2484. https://doi.org/10.4236/am.2014.516239.

Ao, P., 2004. Potential in stochastic differential equations: novel construction. *J. Phy. A Math. Gen*. 37 L25-L30. https://doi.org/10.1088/0305-4470/37/3/L01.

Aris, R., 1965. Introduction to the analysis of chemical reactor. Prentice-Hall, Englewood Cliffs, New Jersey.

Aris, R., 1999. Mathematical Modeling. A Chemical Engineer's Perspective. Academic Press, London (UK).

Balzano, A., Tronci, S., Baratti, R., 2010. Accurate and efficient solution of distributed dynamical system models. *Computer-Aided Chem. Eng*. 28, 421-426. https://doi.org/10.1016/S1570-7946(10)28071-9.

Baratti, R., Tronci, S., Schaum, A., Alvarez, J., 2018. Open and closed-loop stochastic dynamics of a class of nonlinear chemical processes with multiplicative noise. *J. of Proc. Contr*. 21, 108-121. https://doi.org/10.1016/j.jprocont.2018.03.004.

Bashkirtseva, I., Pisarchik, A.N., 2018. Stochastic Analysis and control in kinetics of multistable chemical reactor. *IFAC-PapersOnLine*, 51, 545-549. https://doi.org/10.1016/j.ifacol.2018.11.479.

Bashkirtseva, I., 2018. Controlling the stochastic sensitivity in thermochemical systems. *Kybernetika*, 54(1), 96-109. https://doi.org/10.14736/kyb-2018-1-0096.

Boyce, W. E., Di Prima, R.C., 1967. Elementary differential equations and boundary value problems. John Wiley & Sons, New York.

Burr, I.W., 1976. Statistical quality control methods. Routledge, New York.

Doraiswamy, L.K., Kulkarni, B.D., 1986. Relevance of stochastic modeling in chemically reacting systems. *Ind. Eng. Chem. Fundam*. 25, 511-517. https://doi.org/10.1021/i100024a010.

Franco-de los Reyes, H.A., Schaum, A., Meurer, T., Alvarez, J., 2020. Stabilization of an unstable tubular reactor by nonlinear passive output feedback control. *J. of Proc. Contr*. 93, 83–96. https://doi.org/10.1016/j.jprocont.2020.07.005.

Franco-de los Reyes, H. A., Alvarez, J., 2022. Saturated output-feedback control and state estimation of a class of exothermic tubular reactors. *J. of Proc. Contr*. 93, 78-95. https://doi.org/10.1016/j.jprocont.2022.02.005.

Frank, T.D., 2006. Nonlinear Fokker-Planck equations: fundamentals and applications. Springer Berlin, Heidelberg.

Gardiner, C.W., 1997. Handbook of stochastic methods. Springer-Verlag, Germany.

Gavalas, G.R., 1968. Nonlinear differential equations of chemically reacting systems. Springer-Verlag, New York.

Giona, M., Paladino, O., 1994, Bifurcation analysis and stability of controlled CSTR. *Comp. Chem. Eng*. 18(9), 877-887. https://doi.org/10.1016/0098-1354(94)E0005-8.

Gonzalez, P., Alvarez J., 2005. Combined proportional/integral–inventory control of solution homopolymerization reactors. *Ind. Eng. Chem. Res*. 44(18), 7147–7163. https://doi.org/10.1021/ie040207r.

Hirschorn R.M., 1979. Invertibility nonlinear control systems. *SIAM J. Control Optim*. 17. 289–297. https://doi.org/10.1137/0317022.

Hirsch, M.W., Smale, S., 1974. Differential Equations, Dynamical Systems and Linear Algebra. Academic Press Inc., London.

Hubbard, J.H., West, B.H., 1995. Differential equations: a dynamical systems approach. Springer-Verlag, New York.

Jazwinsky, A.H., 1970. Stochastic processes and filtering theory. Academic Press, New York.

Khalil, H., 2002. Nonlinear systems. Prentice Hall, New Jersey.

Krstic, M., Deng, H., 1988. Stabilization of nonlinear uncertain systems Springer-Verlag, London.

Kwakernaak, K., Sivan, R., 1972. Linear optimal control systems. John Wiley & Sons, Inc. New York.

Kwon, C., Ao, P., Thouless, D.J., 2005. Structure of stochastic dynamics near fixed points. *PNAS* 102, 13029-13033. https://doi.org/10.1073/pnas.0506347102.

Isidori, A., 1999. Nonlinear control systems II. Springer-Verlag.

La Salle, J., Lefschetz, S., 1961. Stability by Liapunov's direct method with applications. Academic Press, New York.

LeVeque, R.J., 1992. Numerical Methods for Conservation Laws. ETH Lectures in Mathematics Series, Birkhauser-Verlag.

Lu, Y., Fang, Z., Gao, C., Dochain, D., 2022. Noise-to-state exponentially stabilizing (state, input)-disturbed CSTRs. *Automatica* 142, 110387. https://doi.org/10.1016/j.automatica.2022.110387.

Mandur, J., Budman, H., 2014. Robust optimization of chemical processes using Bayesian description of parametric uncertainty. *J. of Proc. Contr*. 24, 422-430. https://doi.org/10.1016/j.jprocont.2013.10.004.

Markowich, P. A., Villani, C., 2000. On the trend to equilibrium for the Fokker-Planck equation: an interplay between physics and functional analysis, *Matematica Contemporanea* 19, 1-29. http://doi.org/10.21711/231766362000/rmc191.

Maxim, A., Copot, D., Copot, C., Ionescu, C.M., 2019. The 5w's for control as part of industry 4.0: Why, what, where, who, and when—A PID and MPC control perspective. *Inventions*, 4(1), 10. https://doi.org/10.3390/inventions4010010.

McAvoy, T., 2002. Model predictive statistical process control of chemical plants. *Ind. Eng. Chem. Res*. 41(25). 6337–6344. https://doi.org/10.1021/ie020067q.

Papoulis, A., Unnikrishna Pillai, S., 2002. Probability, Random Variables, and Stochastic Processes. McGraw-Hill, Europe.

Pell, T.M., Aris, R., 1969. Some problems in chemical reactor analysis with stochastic features, Ind. Eng. Chem. Fundam. 8 (1969) 339-345. https://doi.org/10.1021/i160030a026.

Oates, G.C., 1974. Vector Analysis (Ch 3). in Applied Mathematics (Editor: C.E. Pearson), Van Nostrand Reinhold, New York.

Ratto, M., 1998. A theoretical approach to the analysis of PI-controlled CSTRs with noise. *Comp. Chem. Eng*. 22(11), 1581-1593. https://doi.org/10.1016/S0098-1354(98)00232-4.
Ratto, M., Paladino, O., 2000. Analysis of controlled CSTR models with fluctuating parameters and uncertain parameters. *Chem. Eng. J*. 79, 13-21. https://doi.org/10.1016/S1385-8947(00)00139-X.
Risken, H., 1996. The Fokker-Planck Equation: Methods of Solutions and Applications. Springer-Verlag, Berlin.
Samad, T., 2017. A Survey on Industry Impact and Challenges Thereof. *IEEE Control Systems Magazine* 37(1), 17-18. https://doi.org/10.1109/MCS.2016.2621438.
Schaum, A., Alvarez, J., Lopez-Arenas, T., 2012. Saturated PI control of continuous bioreactors with Haldane kinetics. *Chem. Eng. Sci*. 68, 520-529. https://doi.org/10.1016/j.ces.2011.10.006.
Schaum, A., Tronci, S., Baratti, R., Alvarez, J., 2021. On the dynamics and robustness of the chemostat with multiplicative noise. *IFAC-PapersOnLine* 54(3), 342-347. https://doi.org/10.1016/j.ifacol.2021.08.265.
Sepulchre, R., Janoković, M., Kokotović, P., 2012. Constructive Nonlinear Control. Springer Science & Business Media.
Sontag, E.D., 2008. Input to State Stability: Basic Concepts and Results. in: P. Nistri, G. Stefani (Eds), Nonlinear and Optimal Control Theory, Lecture Notes in Mathematics, Springer, Berlin, Heidelberg, pp. 163-220. https://doi.org/10.1007/978-3-540-77653-6_3.
Uppal, A., Ray, W.H., Poore, B., 1974. On the dynamic behavior of continuous stirred tank reactors. *Chem. Eng. Sci*. 29(4), 967–985. https://doi.org/10.1016/0009-2509(74)80089-8.
Vesterinen, T., Ritala, R., 2005. Bioprocesses and other production processes with multi-stability for method testing and analysis. *Computer-Aided Chem. Eng.* 29, 421-426. https://doi.org/10.1016/S1570-7946(05)80265-2.
Vidyasagar, M., 1993. Nonlinear Systems Analysis. Prentice-Hall, New York.
Wang, J., Huang, B., Xia, X., Sun, Z., 2006. Funneled Landscape Leads to Robustness of Cell Networks: Yeast Cell Cycle. *PLoS Comp. Bio*. 2, 1385-1394. https://doi.org/10.1371/journal.pcbi.0020147.

Appendix A: Hurwitz conditions for deterministic SS stability

The 3x3 Jacobian matrix of the deterministic system (23) at its prescribed SS $\overline{\boldsymbol{x}} =$ (32) is

$$\bar{\boldsymbol{J}} = \begin{bmatrix} \boldsymbol{L}(\bar{y}, k_p) & \boldsymbol{v} \\ \boldsymbol{h}(k_I) & 0 \end{bmatrix}, \quad \bar{\boldsymbol{J}}\text{: (35)}, \quad \boldsymbol{f}\text{: (31)} \tag{A1a}$$

where

$$\boldsymbol{L}(\bar{y}, k_p) = \begin{bmatrix} -l_1(\bar{y}) & -c_1(\bar{y}) \\ c_2(\bar{y}) & -l_2(\boldsymbol{z}, k_p) \end{bmatrix}, \qquad \boldsymbol{v} = \begin{bmatrix} 0 \\ -\eta \end{bmatrix}, \qquad \boldsymbol{h}(k_I) = [0,\ k_I]$$

$$c_1 = (\delta/2) r_1(\bar{y}), \quad c_2 = (\delta/2) r_2(\bar{y}), \qquad r_i(\bar{y}) = [\partial_{x_i} r(x_1, x_2)]_{x_1 = m(\bar{y}), x_2 = \bar{y}}$$

$$l_1(\bar{y}, k_p) = \bar{\theta} + \delta r_1(\bar{y}), \quad l_2(\bar{y}, k_p) = l_{2o}(\boldsymbol{x}) + \eta k_p, \quad l_{2o}(\bar{y}, k_p) = \bar{\theta} + \eta - \frac{\delta}{2} r_2(\bar{y})$$

The characteristic polynomial of $\bar{\boldsymbol{J}}$ (A1) is

$$\lambda^3 + a_1(\bar{y}, k_p)\lambda^2 + a_2(\bar{y}, k_p)\lambda + a_3(\bar{y}, k_I) = 0 \tag{A2a}$$

where

$$a_1(\bar{y}, k_p) = T_{\boldsymbol{L}}(\bar{y}, k_p), \quad a_2(\bar{y}, k_p) = D_{\boldsymbol{L}}(\bar{y}, k_p) + k_I \eta, \qquad a_3(\bar{y}, k_I) = k_I \eta l_1 \tag{A2b-d}$$

$$T_{\boldsymbol{L}}(\bar{y}, k_p) = l_1(\bar{y}) + l_2(k_p), \quad D_{\boldsymbol{L}}(\bar{y}, k_p) = l_1(\bar{y}, k_p) l_2(k_p) + c(\bar{y}), \quad c(\bar{y}) = \frac{\delta^2}{2} r_1(\bar{y}) r_2(\bar{y}) \tag{A2e-g}$$

The Hurwitz stability conditions (34) of Proposition 2 (36) are (Boyce and Di Prima, 1967)

$$s_1 = a_1, \quad s_2 = a_1 a_2 - a_3, \quad s_3 = a_3 \tag{A3a-c}$$

or in detailed form

$$s_1(\bar{y}, k_p) = T_{\boldsymbol{L}}(\bar{y}, k_p),\ \ s_2(\bar{y}, k_I) = k_I \eta l_1(\bar{y}),\ \ s_3(\bar{y}, \boldsymbol{k}) = T_{\boldsymbol{L}}(\bar{y}, k_p) D_{\boldsymbol{L}}(\bar{y}, k_p) + l_2(\bar{y}, k_p)\eta k_I. \quad \text{(A4a-c)}$$

Appendix B: Proof of Proposition 4 (*State mode rate of change*)

Following (Jazwinski, 1970), the time derivation of the null-gradient condition (18b) followed by substitution of the RHS of the FP PDE (39) yields that the state mode rate of change is given by

$$\dot{\boldsymbol{x}}_m = -[(\boldsymbol{\mathcal{H}}\pi)^{-1}\boldsymbol{\nabla}\mathcal{F}]_{\boldsymbol{x}=\boldsymbol{x}_m},\ \ \mathcal{F}\text{: (17a)},\ \ \boldsymbol{\nabla}, \boldsymbol{\mathcal{H}}\text{: (18e)} \quad \text{(B1)}$$

The application of the vector analysis formula (Oates, 1974) (for the divergency of the vector-scalar field product $\boldsymbol{v}\pi$)

$$\boldsymbol{\nabla}\cdot(\boldsymbol{v}\pi) = (\boldsymbol{\nabla}\pi)\cdot\boldsymbol{v} + (\boldsymbol{\nabla}\cdot\boldsymbol{v})\pi$$

to the probability transport-generation operator $\mathcal{F}$ of the FP PDE (39) yields the gradient of $\mathcal{F}$

$$\boldsymbol{\nabla}\mathcal{F} = \boldsymbol{\nabla}[\boldsymbol{\nabla}\cdot((1/2)\boldsymbol{Q}\boldsymbol{\nabla}\pi)] - (\boldsymbol{\mathcal{H}}\pi)\boldsymbol{f} - [\boldsymbol{J}^T + \boldsymbol{I}(\boldsymbol{\nabla}\cdot\boldsymbol{f})]\boldsymbol{\nabla}\pi\ - [\boldsymbol{\nabla}(\boldsymbol{\nabla}\cdot\boldsymbol{f})]\pi,\ \ \boldsymbol{Q}\text{: (14h)},\ \boldsymbol{J}\text{: (A1a)}$$

which at the state mode $\boldsymbol{x}_m$ (where $\boldsymbol{\nabla}\pi = \boldsymbol{0}$) becomes

$$\boldsymbol{\nabla}\mathcal{F}(\pi, \boldsymbol{d}) = \boldsymbol{\nabla}[(1/2)\boldsymbol{\nabla}\cdot(\boldsymbol{Q}\boldsymbol{\nabla}\pi)] - (\boldsymbol{\mathcal{H}}\pi)\boldsymbol{f} - [\boldsymbol{\nabla}(\boldsymbol{\nabla}\cdot\boldsymbol{f})]\pi$$

The substitution of this expression in (B1) followed by arrangement yields the FP PDE-based mode rate of change (48) of Proposition 4. **QED**

Appendix C: Proof of Proposition 5 (*Mode evolutions*)

By the CL deterministic stability property (36), the state [$\tilde{\boldsymbol{x}}_m$: (45c)] and control [$\tilde{u}_m$: (45d)] mode and control evolution deviations of the PDF-dependent ODE system (48) with $\boldsymbol{d} = \bar{\boldsymbol{d}}$ and $\boldsymbol{\varrho}_\pi = \boldsymbol{0}$

$$\dot{\boldsymbol{x}}_m = \boldsymbol{f}(\boldsymbol{x}_m, \bar{\boldsymbol{d}}), \qquad \boldsymbol{x}_m(0) = \boldsymbol{x}_{mo} = \boldsymbol{m}_x(\pi_o)$$

are bounded by

$$|\tilde{\boldsymbol{x}}_m(t)| \le a_x e^{-\lambda_x t}|\tilde{\boldsymbol{x}}_{mo}|^+ \coloneqq s(t), \qquad \tilde{\boldsymbol{x}}_m \coloneqq \boldsymbol{x}_m(t) - \bar{\boldsymbol{x}} \quad \text{(C1a)}$$

$$|\tilde{u}_m(t)| \le k_{\boldsymbol{x}_m}^{\boldsymbol{c}_u} a_x e^{-\lambda_x t}|\tilde{\boldsymbol{x}}_{mo}|^+, \qquad \tilde{u}_m = u_m(t) - \bar{u} \quad \text{(C1b)}$$

or equivalently, by the linear scalar ODE-based form

$$|\tilde{\boldsymbol{x}}_m(t)| \le s(t)\text{:}\ \ \dot{s} = -\lambda_x s,\ \ \boldsymbol{s}_o(0) = s_o = a_x|\tilde{\boldsymbol{x}}_{mo}|^+,\ |\tilde{u}_m(t)| \le k_{\boldsymbol{x}_m}^{\boldsymbol{c}_u} s(t) \quad \text{(C2)}$$

From the application (Gonzalez and Alvarez, 2005, Franco-de los Reyes, 2022) of Lyapunov's Converse Theorem (Vidyasagar, 1993) to (48a) in the light of (C1) and (C2), the mode and control evolution deviations of the PDF-dependent ODE system (48) are bounded as

$$|\tilde{\boldsymbol{x}}_m(t)| \le s(t)\text{:}\ \ \dot{s} = -(\lambda_x - a_x l_{\boldsymbol{x}_m}^{\boldsymbol{\varrho}_\pi})s + (a_x/\lambda_x) l_{\boldsymbol{d}}^{\boldsymbol{f}}|\tilde{\boldsymbol{d}}|^+\text{: } \boldsymbol{s}_o(0) = s_o \quad \text{(C3a)}$$

$$|\tilde{u}_m(t)| \le k_{\boldsymbol{x}_m}^{\boldsymbol{c}_u} s(t),\ \ s_o = a_x|\tilde{\boldsymbol{x}}_{mo}|^+,\ \ \lambda_x > a_x l_{\boldsymbol{x}_m}^{\boldsymbol{\varrho}_\pi},\ \ l_{\boldsymbol{x}_m}^{\boldsymbol{\varrho}_\pi}\text{: (47b)},\ l_{\boldsymbol{d}}^{\boldsymbol{f}}\text{: (38d)} \quad \text{(C3b)}$$

From the analytic integration of the linear ODE (C3a) the algebraic bounding inequalities (50) of Proposition 5 follow. **QED**

Appendix D: Stationary state covariance and control variance

D.1 State covariance matrix

In terms of the proportional-integral gain vector $\boldsymbol{k}$ (12), the analytic solution of the stationary Riccati equation (56e) with $\bar{\boldsymbol{\Sigma}} = \bar{\boldsymbol{\Sigma}}_m$ (56b) is given by the state covariance matrix

$$\bar{\boldsymbol{\Sigma}}_m(\boldsymbol{k}) = \begin{bmatrix} \bar{\sigma}_{11} & \bar{\sigma}_{12} & \bar{\sigma}_{13} \\ \bar{\sigma}_{12} & \bar{\sigma}_{22} & \bar{\sigma}_{23} \\ \bar{\sigma}_{13} & \bar{\sigma}_{23} & \bar{\sigma}_{33} \end{bmatrix} = \bar{\boldsymbol{\Sigma}}(\boldsymbol{k}), \quad \boldsymbol{k} \in K_h \subset K, \quad K\text{: (12c)},\ K_h\text{: (36)} \tag{D1}$$

where

$$\bar{\sigma}_{11}(\boldsymbol{k}) = \frac{k_I[2\eta k_I \bar{L}(k_p) + 2\bar{L}(k_p)^2\bar{l}_1 + 2\bar{L}(k_p)\bar{l}_1^2 + \delta^2\bar{l}_1\bar{r}_{x_1}\bar{r}_{x_2}]q_1 + 2\delta^2 k_I\bar{l}_1\bar{r}_{x_2}^2 q_2 + 2\delta^2\eta\bar{r}_{x_2}^2(\bar{L}(k_p)+\bar{l}_1)q_3}{2k_I\bar{l}_1 L_d(\boldsymbol{k})} \tag{D2a}$$

$$\bar{\sigma}_{12}(\boldsymbol{k}) = \frac{\delta k_I\bar{L}(k_p)\bar{r}_{x_1}q_1 + 2\delta k_I\bar{l}_1\bar{r}_{x_2}q_2 - 2\delta\eta\bar{r}_{x_2}(\bar{L}(k_p)+\bar{l}_1)q_3}{2k_I L_d(\boldsymbol{k})} \tag{D2b}$$

$$\bar{\sigma}_{13}(\boldsymbol{k}) = \frac{\delta k_I^2\bar{L}(k_p)\bar{r}_{x_1}q_1 - 2\delta k_I^2\bar{l}_1\bar{r}_{x_2}q_2 + \delta[\bar{r}_{x_2}(\bar{L}(k_p)+\bar{l}_1)(2\bar{L}(k_p)\bar{l}_1 + \delta^2\bar{r}_{x_1}\bar{r}_{x_2}) - 2\eta k_I\bar{l}_1\bar{r}_{x_2}]q_3}{2k_I\bar{l}_1 L_d(\boldsymbol{k})} \tag{D2c}$$

$$\bar{\sigma}_{22}(\boldsymbol{k}) = \frac{\delta^2 k_I\bar{r}_{x_1}^2 q_1 + 2k_I[2\eta k_I + 2\bar{L}(k_p)\bar{l}_1 + 2\bar{l}_1^2 + \delta^2\bar{r}_{x_1}\bar{r}_{x_2}]q_2 + 4[\eta^2 k_I + \eta\bar{L}(k_p)\bar{l}_1 + \eta\bar{l}_1^2]q_3}{4k_I L_d(\boldsymbol{k})} \tag{D2d}$$

$$\bar{\sigma}_{23}(\boldsymbol{k}) = -\frac{q_3}{2k_I}, \qquad \bar{\sigma}_{33}(\boldsymbol{k}) = \frac{\delta^2 k_I^2\bar{r}_{x_1}^2(\bar{L}(k_p)+\bar{l}_1)q_1 + 4k_I^2\bar{l}_1[\eta k_I + \bar{L}(k_p)\bar{l}_1 + \bar{l}_1^2]q_2 + \beta_1 q_3 + \beta_2 q_c}{4\eta k_I\bar{l}_1 L_d(\boldsymbol{k})} \tag{D2e-f}$$

and

$q_1, q_2(k_p), q_3(k_I), q_c(\boldsymbol{k})$: (14h)

$$L_d(\boldsymbol{k}) = \{2\eta k_I\bar{L}(k_p) + [\bar{L}(k_p) + \bar{l}_1][2\bar{L}(k_p)\bar{l}_1 + \delta^2\bar{r}_{x_1}\bar{r}_{x_2}]\}$$

$$\beta_1(\boldsymbol{k}) = 4\eta k_I\bar{l}_1[\eta k_I + \bar{L}(k_p)^2 + \bar{L}(k_p)\bar{l}_1 + \bar{l}_1^2] + 4\bar{L}(k_p)\bar{l}_1(\bar{L}(k_p)^2 + \bar{l}_1^2) + \delta^2[4\bar{L}(k_p)\bar{l}_1(\bar{L}(k_p) + \bar{l}_1) - 2\eta k_I\bar{l}_1 + \delta^2(\bar{L}(k_p) + \bar{l}_1)\bar{r}_{x_1}\bar{r}_{x_2}]\bar{r}_{x_1}\bar{r}_{x_2}$$

$$\beta_2(\boldsymbol{k}) = 4k_I\bar{l}_1[2\eta k_I\bar{L}(k_p) + 2\bar{L}(k_p)^2\bar{l}_1 + 2\bar{L}(k_p)\bar{l}_1^2 + \delta^2(\bar{L}(k_p) + \bar{l}_1)\bar{r}_{x_1}\bar{r}_{x_2}]$$

D.2 Marginal state and control PDFs

Knowing the stationary solution of the covariance matrix, it is possible compute the marginal PDFs for concentration (μ_{x_1}), temperature (μ_{x_2}) and integral action (μ_{x_3}) from the approximated steady state PDF (41)

$$\hat{\mu}_{x_1}(x_1, \boldsymbol{k}) = \frac{1}{\sqrt{2p_n\bar{\sigma}_{11}(\boldsymbol{k})}}\exp\left[-\frac{(x_1-\bar{x}_1)^2}{2\bar{\sigma}_{11}(\boldsymbol{k})}\right], \quad \bar{\sigma}_{11}(\boldsymbol{k})\text{: (D2a)} \tag{D3a}$$

$$\hat{\mu}_{x_2}(x_2, \boldsymbol{k}) = \frac{1}{\sqrt{2p_n\bar{\sigma}_{22}(\boldsymbol{k})}}\exp\left[-\frac{(x_2-\bar{x}_2)^2}{2\bar{\sigma}_{22}(\boldsymbol{k})}\right], \quad \bar{\sigma}_{22}(\boldsymbol{k})\text{: (D2d)} \tag{D3b}$$

$$\hat{\mu}_{x_3}(x_3, \boldsymbol{k}) = \frac{1}{\sqrt{2p_n\bar{\sigma}_{33}(\boldsymbol{k})}}\exp\left[-\frac{(x_3-\bar{x}_3)^2}{2\bar{\sigma}_{33}(\boldsymbol{k})}\right], \quad \bar{\sigma}_{33}(\boldsymbol{k})\text{: (D2f)} \tag{D3c}$$

and the unidimensional control ν PDF can be determined through (18f) by (Papoulis and Pillai, 2002)

$$\hat{\nu}(u, \boldsymbol{k}) = \frac{1}{2\sqrt{2p_n\bar{\sigma}_u(\boldsymbol{k})}}\exp\left[-\frac{(u-\bar{x}_3)^2}{2\bar{\sigma}_u(\boldsymbol{k})}\right], \ \bar{\sigma}_u(\boldsymbol{k}) = k_p^2\bar{\sigma}_{22}(\boldsymbol{k}) + \bar{\sigma}_{33}(\boldsymbol{k}), \quad p_n\text{: “pi” number} \tag{D3d}$$

Figure captions

Figure 1. Stationary state PDF [$\bar{\varsigma}(\boldsymbol{z})$ (11a)] behavior regions of the reactor class (3), in the Damköhler-Stanton parameter space delimited by deterministic saddle-node (S_b) (- - - -) and Hopf (H_b) (——) bifurcation: (i) monomodal (white), (ii) bimodal (yellow), and (iii) vulcanoid (pink). Indicative examples (Table 3) (•): (i) C_1 (fragile bimodality), (ii) C_2 (robust bimodality), and (iii) C_3 (robust vulcanoid).

Figure 2. Dependency of the stationary concentration ($\bar{s}_1$) and temperature ($\bar{s}_2$) states as well as control ($\bar{s}_3$) PDF standard deviations on the control gain pair $\boldsymbol{\kappa} \in \mathcal{K}$ (61) for Case C_1 (Table 3) with noise STDs (59a-c). • (in bottom plane): tight control gain $\boldsymbol{\kappa}_1^t \in \mathcal{K}_h$ (63a).

Figure 3. Stationary concentration-temperature state PDFs for Case C_1 (Table 3) with tight control gain $\boldsymbol{\kappa}_1^t$ (63a): (i) OL $\bar{\varsigma}(\boldsymbol{z})$ (11a) (top panel), and (ii) CL marginal $\bar{\varsigma}_c(\boldsymbol{z})$ (62) (bottom panel) of $\bar{\pi}(\boldsymbol{x})$ (41).

Figure 4: CL concentration (μ_{x_1}), temperature (μ_{x_2}) and integral action (μ_{x_3}) state marginal PDF evolutions (18g) of Case C_1 (Table 3) with: (i) tight gain $\boldsymbol{\kappa}_1^t \in \mathcal{K}_h$ (63a) (left column), and (ii) tight gain $\boldsymbol{\kappa}_1^l \in \mathcal{K}_h$ (63b) (right column).

Figure 5: Actual FP PDE (46) (black line) and approximated ODE (54a)-based (blue dashed line) CL concentration, temperature, and integral action state mode evolutions for Case C_1 (Table 3) with: (i) tight gain $\boldsymbol{\kappa}_1^t \in \mathcal{K}_h$ (63a) (left panel), and (ii) loose gain $\boldsymbol{\kappa}_1^l \in \mathcal{K}_h$ (63b) (right panel).

Figure 6. CL concentration (μ_{x_1}), temperature (μ_{x_2}), integral action (μ_{x_3}) and control (ν) state marginal PDF evolutions (18f-g) in contour form (black: mode, yellow/blue: most/least probable) for Case C_1 (Table 3) with tight control gain $\boldsymbol{\kappa}_1^t \in \mathcal{K}_h$ (63a), on the basis of the numerical solutions of: (ii) the Riccati ODE (54) (left panel), and (ii) the FP PDE (39) (right panel).

Figure 7. Dependency of the CL stationary concentration ($\bar{s}_1$) and temperature ($\bar{s}_2$) states as well as control ($\bar{s}_3$) PDF STDs on the control gain pair $\boldsymbol{\kappa} \in \mathcal{K}$ (61) for Case C_2 (Table 3) with noise STDs (60). • (in bottom plane $\mathcal{K}$): control gain $\boldsymbol{\kappa}_2 \in \mathcal{K}_h$ (65).

Figure 8. Stationary concentration-temperature state PDFs for Case C_2 (Table 3) with control gain $\boldsymbol{\kappa}_2 \in \mathcal{K}_h$ (65): (i) OL $\bar{\varsigma}(\boldsymbol{z})$ (11a) (top panel), and (ii) CL marginal $\bar{\varsigma}_c(\boldsymbol{z})$ (62) (bottom panel) of $\bar{\pi}(\boldsymbol{x})$ (41).

Figure 9. Dependency of the CL stationary concentration ($\bar{s}_1$) and temperature ($\bar{s}_2$) states as well as control ($\bar{s}_3$) PDF STDs on the control gain pair $\boldsymbol{\kappa} \in \mathcal{K}$ (61) for Case C_3 (Table 3) with noise STDs (60). • (in bottom plane $\mathcal{K}$): control gain $\boldsymbol{\kappa_3} \in \mathcal{K}_h$ (66).

Figure 10. Stationary concentration-temperature state PDFs for Case C_3 (Table 3) with control gain $\boldsymbol{\kappa}_3$ (66): (i) OL $\bar{\varsigma}(\boldsymbol{z})$ (11a) (top panel), and (ii) CL marginal $\bar{\varsigma}_c(\boldsymbol{z})$ (62) (bottom panel) of $\bar{\pi}(\boldsymbol{x})$ (41).